Pinning-Based Hierarchical and Distributed Cooperative Control for AC Microgrid Clusters

Xiangyu Wu, *Member, IEEE*, Yin Xu, *Senior Member, IEEE*, Jinghan He, *Fellow, IEEE*, Xiaojun Wang, *Member, IEEE*, Juan C. Vasquez, *Senior Member, IEEE*, and Josep M. Guerrero, *Fellow, IEEE*

***Abstract*—With the large-scale application of microgrids (MGs), interconnecting nearby MGs to form an MG cluster (MGC) enables a higher utilization of renewable sources. This article presents a pinning-based hierarchical and distributed cooperative control strategy for AC MGC, which includes distributed generation (DG)-layer, MG-layer, and MGC-layer controls. The DG-layer control regulates the local voltage/current of each DG unit. The MG-layer control is performed for each individual MG, managing DG units in a cooperative manner through several sparse communication networks. By representing each MG as an MG agent, the MGC-layer control coordinates MGs based on a higher level peer-to-peer communication network among MG agents. The interaction between MG-layer and MGC-layer is established by pinning some DG units of each MG to communicate with the MG agent. Compared with the existing literature, the contributions of this article are: 1) simultaneously realizing multiple control objectives in the MGC system level including frequency/voltage regulation and active/reactive power sharing; 2) presenting a systematic approach to construct a unified small-signal dynamic model of the MGC system; and 3) performing a detailed small-signal stability analysis to evaluate the system dynamic performance. Time-domain simulation and experiments are carried out to validate the effectiveness of the proposed methods.**

***Index Terms*—Distributed cooperative control, dynamic model, hierarchical control, microgrid cluster (MGC), small-signal stability.**

I. Introduction

MICROGRID (MG) is a viable technical option to systematically organize the distributed generation (DG) units and facilitate their local consumption [1]–[3]. With the large-scale development of MGs, a number of adjacent MGs could be connected together to form an MG cluster (MGC) in a certain region [4], [5]. Because of the power support capability among different MGs, the MGC can further promote the utilization of renewable sources and also enhance the system resiliency after major disasters [6]–[8].

A desirable control system is of vital importance for an MGC to ensure its stable and efficient operation. First, compared with a single MG, the MGC not only needs to consider the control of DG units inside each individual MG, but also ought to realize the coordination control among different MGs. Second, multiple control objectives both in the individual MG level and in the whole system level need to be realized for an MGC. Therefore, considering that each MG can be regarded as a control area, the MGC control is a kind of multi-area, multi-layer, and multi-objective control problem, which is extremely challenging.

One strategy to realize the MGC control is the centralized control method, which requires a central control unit and bidirectional communication links between the central control unit and each control device. In [9]–[12], a system central controller is employed for coordinating each DG unit in the MGC to realize the system frequency/voltage/power control objectives. However, the centralized method suffers from the problem of "single point of failure" for the central control unit, which significantly decrease the system reliability and scalability [13].

In contrast, the distributed control method does not rely on the central control unit. It is based on a sparse communication network in which each control device requires its own information and that of its neighbors to perform control actions [14]. The distributed control method has been widely studied in a single MG [13], [15]–[18]. For the application of distributed control in the MGC, relevant works are summarized as follows.

Amoateng *et al.* [19] and Golsorkhi *et al.* [20] proposed a distributed control method to realize the control of system frequency, DG units output voltages or power sharing among DG units in the MGC. However, all the DG units from different MGs are in the same communication network. This is similar to control "a large MG" and, thus, it breaks the autonomy characteristic of each MG as an area, which may result in problems of privacy protection, slow algorithm convergence speed, and difficulties in the MG plug-and-play [21], [22]. To overcome this drawback, Moayedi *et al.* [23] and Shafiee *et al.* [24] introduced an MG agent for each MG. The MG agents communicate with each other to achieve the coordination among different MGs. For the DG units, only DG units from the same MG have communications. This method can reserve the autonomy characteristic of MGs, however, the control methods in [23] and [24] are

Manuscript received August 19, 2019; revised December 25, 2019; accepted January 30, 2020. Date of publication February 7, 2020; date of current version May 1, 2020. This work was supported in part by the National Key R&D Program of China under Grant 2018YFB0905200, in part by the National Natural Science Foundation of China under Grant 51807005. The work of J. M. Guerrero was funded by a Villum Investigator under Grant 25920 from The Villum Fonden. Recommended for publication by Associate Editor G. Oriti. *(Corresponding author: Yin Xu.)*

Xiangyu Wu, Yin Xu, Jinghan He, and Xiaojun Wang are with the School of Electrical and Engineering, Beijing Jiaotong University, Beijing 100044, China (e-mail: wuxiangyu@bjtu.edu.cn; xuyin@bjtu.edu.cn; jhhe@bjtu.edu.cn; xjwang1@bjtu.edu.cn).

Juan C. Vasquez and Josep M. Guerrero are with the Center of Research on Microgrids (CROM), Department of Energy Technology, Aalborg University, 9220 Aalborg East, Denmark (e-mail: juq@et.aau.dk; joz@et.aau.dk).

Color versions of one or more of the figures in this article are available online at http://ieeexplore.ieee.org.

Digital Object Identifier 10.1109/TPEL.2020.2972321

designed for DC MGC rather than AC MGC. For AC MGC, Wu *et al.* [21] introduced an interface controller to mimic the droop characteristic for each MG, while the newly introduced controller increases the implementation complexity. In addition, Wu *et al.* [21] aimed to share the output power from the point of common coupling (PCC) of each MG in proportion to the capacities of MGs. However, it will result in no power support among MGs when all the loads are inside MGs. In [22] and [25], the concept of MG agent [22] or DG-head [25] (similar to MG agent) is introduced for AC MGC and corresponding distributed control methods are proposed, which can realize power support among MGs regardless of load positions. However, the studies by Lu and Lai *et al.* [22], [25] have the following limitations.

1) The active power sharing among DG units is in proportion to their capacities. However, an economic operation of the MGC system, e.g., minimization of generation costs, is usually more desirable from the perspective of overall system operation, which cannot be realized in [22] and [25].
2) In [22] and [25], the average value of DG unit output voltages is controlled at the set value. However, actually, the voltages of critical buses in the system should be controlled to ensure continuous operation of sensitive loads and facilitate the synchronization of MGC system to the main grid or the synchronization of sub-MG to the MGC system.
3) The validation of control methods in [22] and [25] is based on time-domain simulations rather than experiments.

Moreover, stability performance is another important concern for the reliable operation of an MGC system. The studies by Lu and Lai *et al.* [22], [25] provided the MGC system stability analysis results based on the Lyapunov-based method. However, the Lyapunov-based method cannot provide the information of damping and oscillation frequency. In addition, it suffers from the problem of conservativeness for the stability analysis result, which may result in undesirable errors. In contrast, the eigenvalue-based small-signal stability analysis can provide many insights on the system dynamics. A small-signal dynamic model can be used for analyzing the system small-signal stability and tuning control parameters. Although the small-signal dynamic model of a single MG is well established [26]–[30], to the best of our knowledge, a small-signal dynamic model for the AC MGC system and the corresponding detailed stability analysis have less been studied before. Compared with a single MG, the modeling of an MGC system is more complicated, since it needs to consider the interconnection of MGs and the multi-area/multi-layer controllers.

Motivated by the aforementioned limitations, this article presents a pinning-based hierarchical control strategy for islanded AC MGC based on the distributed cooperative control theory. The control strategy consists of three layers, i.e., DG-layer control, MG-layer control to manage DG units inside each individual MG, and MGC-layer control to coordinate MGs. The major contributions of this article are threefolds.

1) Compared with the existing MGC control methods, the proposed method can simultaneously: a) realize an economic operation of the system by minimizing the overall generation cost; b) provide the voltage control capability for the system critical bus and the PCC of each MG; c) restore the system frequency to the desired (rated) values; and d) achieve an accurate reactive power sharing among DG units.
2) A systematic approach to modeling the MGC system is presented. The constructed small-signal dynamic model considers the modules of DGs and MGs with the proposed three-layer distributed controllers, lossy-line networks, and loads. All the modules are combined to be a unified model.
3) A detailed small-signal stability analysis for the MGC system is carried out. The relationship between the dominant oscillation modes and key state variables/controllers is established. General guidelines for tuning control parameters are also provided.

The remainder of this article is organized as follows. Section II presents the three-layer distributed control framework of MGC system. Section III elaborates the proposed control method. Section IV develops the small-signal dynamic model of MGC system. Numerical results including stability analysis and time-domain simulation are presented in Section V. Section VI provides the experimental results. Finally, Section VII concludes the article.

II. Three-Layer Distributed Control Framework of MGC

A. Control Framework

Assume that there are M MGs in the MGC system, labeled as $\mathrm{MG}_1, \ldots, \mathrm{MG}_k, \ldots, \mathrm{MG}_M$. There are N_k DG units in MG_k, $k = 1, 2, \ldots, M$. Fig. 1 shows the three-layer distributed control framework of MGC in this article, which includes the DG-layer, MG-layer, and MGC-layer.

1) DG-layer: The DG-layer control is responsible for regulating the local voltage and current of each DG unit in a decentralized manner, i.e., there are no communications among DG units in this layer. The droop-based control [1] has been identified as an effective decentralized control approach for the DG-layer.
2) MG-layer: The MG-layer control is performed for each MG individually, realizing the coordination of DG units inside MG in a distributed manner. Each MG has a distributed sparse communication network (*lower* communication network) among DG units to achieve a cooperative control. The MG-layer control of each MG is usually used for allocating internal DG units' power and tracking the MG voltage and frequency references dictated by the MGC-layer.
3) MGC-layer: In the MGC-layer, each MG is represented as an MG agent. Each MG agent communicates with its neighbors to form a distributed *upper* communication network. In each MG, at least one DG unit is selected as the *pinned* DG unit, which has a bidirectional communication link (*pinning* link) to the corresponding MG agent. Through the pinning links, the MG agent collects the needed information from the pinned DG units and

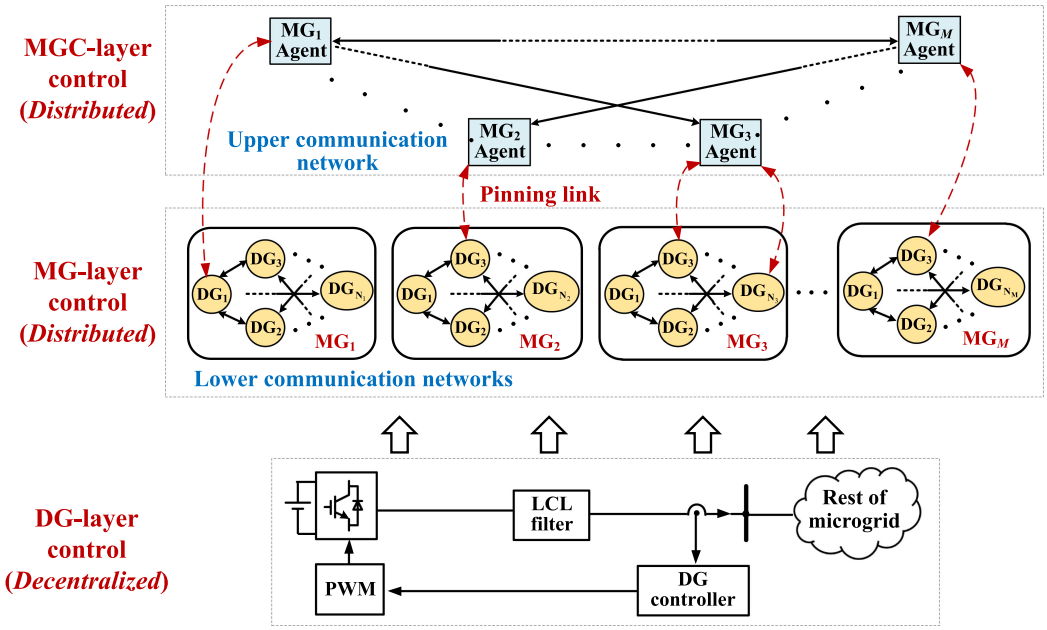

Fig. 1. Three-layer distributed cooperative control framework of MGC.

also sends references to the pinned DG units, realizing the interaction between MGC-layer and MG-layer. The MGC-layer control should coordinate each MG to share active/reactive power among them and also regulate the system frequency and voltage in a distributed manner.

B. Double-Layer Cyber Network Modeling

The lower communication networks in the MG-layer can be modeled as M directed graphs (digraphs) $G_1, \ldots, G_k, \ldots, G_M$ corresponding to each MG. For DG_i in MG_k, the set of its neighbors is denoted as $\mathcal{N}_i^k, i = 1, 2, \ldots, N_k$. The associated adjacency matrix of G_k is defined as $\mathcal{A}^k = [a_{ij}^k]_{N_k \times N_k}$, where a_{ij}^k is the weight of the communication link from DG_j to DG_i.

The upper communication network among MGs in the MGC-layer can be modeled as a digraph $\widetilde{G}$. The set of neighbors of MG_k is denoted as $\mathcal{H}^k, k = 1, 2, \ldots, M$. The associated adjacency matrix of $\widetilde{G}$ is defined as $\widetilde{\mathcal{A}} = [\tilde{a}_{kl}]_{M \times M}$, where $\tilde{a}_{kl}$ is the weight of the communication link from MG_j to MG_i.

To model the pinning links between upper and lower cyber networks, we introduce the leader-adjacency matrix $\mathcal{B}_{\mathrm{pin}}^k = [g_1^k, g_2^k, \ldots, g_{N_k}^k]$ for each MG_k. The pinning gain $g_i^k = 1$ if DG_i is the pinned DG unit; otherwise $g_i^k = 0$.

More details about the graph theory can be referred to [13].

C. Basic Principle of Distributed Cooperative Control Theory

In this article, the distributed cooperative control theory [14] is employed to design controllers in the MG-layer and MGC-layer. Based on the sparse communication network modeled by a digraph, its basic principle is illustrated as follows.

Assume that each node i has a scalar information state x_i. Node i needs information of its own and that of its neighbors j ($j \in \mathcal{N}_i$) to update its state, where $\mathcal{N}_i$ is the set of its neighbors. Based on the continuous consensus algorithm, the update rules can be categorized as synchronization problem in (1) and tracking problem in (2), where a_{ij} is the element of the associated adjacency matrix, and g_i is the pinning gain

$$\dot{x}_i(t) = -\sum_{j \in \mathcal{N}_i} a_{ij}(x_i(t) - x_j(t)) \tag{1}$$

$$\dot{x}_i(t) = -\sum_{j \in \mathcal{N}_i} a_{ij}(x_i(t) - x_j(t)) - g_i(x_i(t) - x_{\mathrm{ref}}). \tag{2}$$

If the communication network has a spanning tree [14], then: 1) for (1), the states x_i of all the nodes will synchronize to a consensus value; and 2) for (2), x_i of all the nodes will track the reference value x_{ref}. In sum, (1) is a synchronization-based algorithm in which the consensus value is not prescribed, while (2) is a tracking-based algorithm in which x_{ref} is assigned to the pinned nodes to realize the reference tracking. It should be noted that x_{ref} could also have dynamics.

III. Pinning-Based Hierarchical and Distributed Cooperative Control Method

Based on the three-layer control framework in Section II, this section presents detailed control strategies for each layer.

A. DG-Layer Control

The droop-based control is adopted in this layer for each DG unit, which includes the power controller, voltage controller, and current controller [1]. The power controller is responsible for obtaining the frequency and voltage reference of DG units based on the power droop characteristics, given by

$$\omega_{ki} = \omega_n - m_{ki}(P_{ki} - P_{ki}^*) \tag{3}$$

$$|v_{oki}^*| = V_{0\alpha} - n_{ki}Q_{ki} \tag{4}$$

where the subscript "ki" corresponds to DG_i in MG_k (i.e., DG_{ki}), ω_{ki} and v^*_{oki} are the frequency and output voltage reference of DG_{ki}, ω_n is the system rated frequency ($2\pi \times 50$ rad/s), $V_{0\alpha}$ is the no-load voltage, and $m_{ki}, n_{ki}, P_{ki}, Q_{ki}, P^*_{ki}$ are the active and reactive power droop coefficients, output active and reactive power, and rated active power of DG_{ki}, respectively. Then, the voltage and current controllers enable a closed-loop regulation of DG unit output voltage v_{oki} to its reference value v^*_{oki}.

The traditional active power droop controller (3) shares the active power among DG units based on the ratios of their capacities. However, an economic operation of the system cannot be guaranteed with this kind of power sharing scheme. Instead of (3), we adopt an optimal active power droop control method in this article, which can share the active power among DG units such that the system overall generation cost is minimized.

The generation cost function of DG_{ki} is denoted as $\mathrm{GC}_{ki}(P_{ki})$. Thus, the overall generation cost minimization problem, i.e., economic dispatch (ED) problem, in MG_k can be formulated as

$$\begin{aligned} \min \quad & \sum_{i=1}^{N_k} \mathrm{GC}_{ki}\left(P_{ki}\right) \\ \text{s.t.} \quad & \sum_{i=1}^{N_k} P_{ki} = P_{\mathrm{Load}} \end{aligned} \tag{5}$$

where P_{Load} is the total load power in MG_k. The Lagrange multiplier method can be used to solve the optimization problem in (5). The Lagrange function L_{ag} is constructed as

$$L_{ag} = \sum_{i=1}^{N_k} \mathrm{GC}_{ki}\left(P_{ki}\right) + \eta\left(P_{\mathrm{Load}} - \sum_{i=1}^{N_k} P_{ki}\right) \tag{6}$$

where η is the Lagrange multiplier. According to the optimality conditions, we have

$$\frac{\partial L_{ag}}{\partial P_{ki}} = \frac{\partial GC_{ki}\left(P_{ki}\right)}{\partial P_{ki}} - \eta = 0, \quad i = 1, 2, \ldots, N_k. \tag{7}$$

$\frac{\partial GC_{ki}(P_{ki})}{\partial P_{ki}}$ is the generation cost increment value (GCIV) of DG_{ki}, which can be denoted as $\eta_{ki}(P_{ki})$. Then, from (7), we have

$$\eta_{k1}(P_{k1}) = \eta_{k2}(P_{k2}) = \cdots = \eta_{kN_k}(P_{kN_k}). \tag{8}$$

Equation (8) is the equal increment principle (EIP) of ED problem to minimize the overall generation cost. Thereafter, the optimal active power droop equation can be designed as

$$\omega_{ki} = \omega_n - k_{ed}\eta_{ki}(P_{ki}) \tag{9}$$

where k_{ed} is a positive scalar coefficient. In the steady state, ω_{ki} of all the DG units must be equal [26], and, thus, $\eta_{ki}(P_{ki})$ are also equal from (9), i.e., (8) is satisfied. Therefore, the system overall generation cost can be minimized with (9).

In sum, (4) and (9) are the active/reactive power droop controllers used in this article for the DG-layer control.

B. MG-Layer Control

For MG_k, the objectives of the MG-layer control are as follows.

1) (MG-i): Enabling each DG unit's frequency track the reference value $\omega_{\mathrm{ref}k}$ from the MGC-layer, while maintaining the EIP (8) achieved in the DG-layer control.
2) (MG-ii): Enabling each DG unit's intermediate voltage V_{fk} (defined later) track the reference value $V_{f\mathrm{ref}k}$ from the MGC-layer, while realizing an accurate reactive power sharing among DG units based on their capacities, i.e.

$$n_{k1}Q_{k1} = n_{k2}Q_{k2} = \cdots = n_{kN_k}Q_{kN_k}. \tag{10}$$

Based on the lower communication network G_k, the frequency and voltage controllers of MG_k can be designed according to the distributed cooperative control theory.

1) MG-Layer Frequency Controller: The frequency controller in the MG-layer is responsible for realizing objective (MG-i), given by

$$\omega_{ki} = \omega_n - k_{ed}\eta_{ki}(P_{ki}) + \Omega_{ki} \tag{11}$$

$$\begin{aligned} \frac{d\Omega_{ki}}{dt} = & -c_{\omega ki}\left[\sum_{j\in\mathcal{N}_i^k} a_{ij}^k(\omega_{ki} - \omega_{kj}) + g_i^k(\omega_{ki} - \omega_{\mathrm{ref}k})\right] \\ & - c_{Pki}\sum_{j\in\mathcal{N}_i^k} a_{ij}^k\left(k_{ed}\eta_{ki}(P_{ki}) - k_{ed}\eta_{kj}(P_{kj})\right). \end{aligned} \tag{12}$$

Equation (11) is transformed from (9) with an additional shift variable Ω_{ki}. In (12), Ω_{ki} is determined based on a combination of tracking problem (2) and synchronization problem in (1), where $c_{\omega ki}$ and c_{Pki} are positive control gains, and $\omega_{\mathrm{ref}k}$ is the frequency reference value for MG_k from the MGC-layer. $\omega_{\mathrm{ref}k}$ is sent to the pinned DG units through pinning links. The dynamic process of (12) results in ω_{ki} of all DG units in MG_k converging to $\omega_{\mathrm{ref}k}$ and the realization of (8).

Remark 1: The transients of $\omega_{\mathrm{ref}k}$ of different MGs could be different to adjust the power flow of MG. However, they will be synchronized to a common value in the steady state by the MGC-layer controller as illustrated in Section III-C.

2) MG-Layer Voltage Controller: The voltage controller in the MG-layer is responsible for realizing objective (MG-ii), given by

$$v^*_{odki} = \underbrace{V_n - n_{ki}Q_{ki} + \lambda_{ki}}_{V_{fki}} - h_{ki} \tag{13a}$$

$$v^*_{oqki} = 0 \tag{13b}$$

where v^*_{odki} and v^*_{oqki} are, respectively, the d-axis and q-axis components of v^*_{oki}. Equation (13a) is transformed from (4) with two additional shift variables λ_{ki} and h_{ki}. Note that $V_n - n_{ki}Q_{ki} + \lambda_{ki}$ is denoted as an intermediate voltage variable V_{fki}, and v^*_{oqki} is set to zero.

λ_{ki} is determined based on the tracking problem (2), given by

$$\frac{d\lambda_{ki}}{dt} = -c_{vki}\left[\sum_{j\in\mathcal{N}_i^k} a_{ij}^k(V_{fki} - V_{fkj}) + g_i^k(V_{fki} - V_{f\mathrm{ref}k})\right] \tag{14}$$

where c_{vki} is a positive control gain. $V_{f\mathrm{ref}k}$ is the intermediate voltage reference for MG_k from the MGC-layer, which is sent to the pinned DG units through pinning links. The dynamic process of (14) will result in V_{fki} of all DG units in MG_k converging to $V_{f\mathrm{ref}k}$.

h_{ki} is determined based on the synchronization problem (1), given by

$$\frac{dh_{ki}}{dt} = c_{Qki} \sum_{j\in\mathcal{N}_i^k} a_{ij}^k (n_{ki}Q_{ki} - n_{kj}Q_{kj}) \tag{15}$$

where c_{Qki} is a positive control gain. The dynamic process of (15) will impose $n_{k1}Q_{k1} = n_{k2}Q_{k2} = \cdots = n_{kN_k}Q_{kN_k}$ in the steady state.

Remark 2: Since the consensus regulation of DG output voltages and an accurate reactive power sharing is contradictory [15], this article preferentially chooses to realize an accurate reactive power sharing. Therefore, in (14), the intermediate voltage V_{fki}, rather than the actual output voltage, is regulated to the consensus value $V_{f\mathrm{ref}k}$.

C. MGC-Layer Control

The MGC-layer control determines $\omega_{\mathrm{ref}k}$ and $V_{f\mathrm{ref}k}$ for each MG. The objectives of this layer are as follows.

1) (MGC-i): Restoring the system frequency to the predefined value ω_{sys}^* while ensuring an equal GCIV among pinned DG units of all MGs.
2) (MGC-ii): Restoring the system critical bus voltage V_{cri} to the predefined value V_{cri}^*, providing the voltage control capability for the PCC voltage of each MG, and realizing an accurate reactive power sharing among pinned DG units of all MGs.

Without loss of generality, ω_{sys}^* and V_{cri}^* are chosen as the rated frequency and voltage values in this article.

Based on the upper communication network $\widetilde{G}$ among MG agents, the MGC-layer controllers can also be designed based on the distributed cooperative control theory.

To facilitate the controller design, we first define two new variables $\eta_{k,\mathrm{pin}}$ and $\mathcal{Q}_{k,\mathrm{pin}}$. From Fig. 1, each MG agent collects information from the pinned DG units through pinning links. Denote $\mathcal{F}^k$ as the set of pinned DG units in MG_k, and $|\mathcal{F}^k|$ is the cardinality of $\mathcal{F}^k$. Then, $\eta_{k,\mathrm{pin}}$ and $\mathcal{Q}_{k,\mathrm{pin}}$ are defined as

$$\eta_{k,\mathrm{pin}} = \frac{1}{|\mathcal{F}^k|} \sum_{i\in\mathcal{F}^k} \eta_{ki}(P_{ki}),\ k = 1, 2, \ldots, M \tag{16}$$

$$\mathcal{Q}_{k,\mathrm{pin}} = \frac{1}{|\mathcal{F}^k|} \sum_{i\in\mathcal{F}^k} n_{ki}Q_{ki},\ k = 1, 2, \ldots, M. \tag{17}$$

From (16) and (17), $\eta_{k,\mathrm{pin}}$ and $\mathcal{Q}_{k,\mathrm{pin}}$ are the average values of $\eta_{ki}(P_{ki})$ and $n_{ki}(Q_{ki})$ of all the pinned DG units in MG_k, respectively.

Moreover, at least one MG agent needs to be pinned to receive the system reference value, e.g., ω_{sys}^*. The pinning gain $\tilde{g}_k = 1$ if MG_k agent is pinned; otherwise, $\tilde{g}_k = 0$.

1) MGC-Layer Frequency Controller: The frequency controller in the MGC-layer is responsible for realizing objective (MGC-i), given by

$$\omega_{\mathrm{ref}k} = \omega_n + \Phi_k \tag{18}$$

$$\frac{d\Phi_k}{dt} = -c_{\omega k}\left[\sum_{l\in\mathcal{H}^k} \tilde{a}_{kl}(\omega_{\mathrm{ref}k} - \omega_{\mathrm{ref}l}) + \tilde{g}_k(\omega_{\mathrm{ref}k} - \omega_{\mathrm{sys}}^*)\right] - c_{Pk}\sum_{l\in\mathcal{H}^k} \tilde{a}_{kl}\,(k_{ed}\eta_{k,\mathrm{pin}} - k_{ed}\eta_{l,\mathrm{pin}}). \tag{19}$$

From (18), $\omega_{\mathrm{ref}k}$ is the sum of the rated frequency ω_n and a regulation variable Φ_k. From (19), Φ_k is determined based on a combination of tracking problem in (2) and synchronization problem in (1), where $c_{\omega k}$ and c_{Pk} are positive control gains. The dynamic process of (19) will result in $\omega_{\mathrm{ref}k}$ of all MGs converging to ω_{sys}^* and $\eta_{k,\mathrm{pin}}$ of all MGs being equal with each other.

2) MGC-Layer Voltage Controller: The voltage controller in the MGC-layer is responsible for realizing objective (MGC-ii), given by

$$V_{\mathrm{PCC}k}^* = \underbrace{V_{0\beta} + T_k}_{V_{sk}} - H_k \tag{20}$$

where $V_{\mathrm{PCC}k}^*$ is the reference value for the PCC voltage $V_{\mathrm{PCC}k}$ of MG_k, $V_{0\beta}$ is a voltage constant (normally set around rated voltage), T_k and H_k are two regulation variables. Note that $V_n + T_k$ is denoted as V_{sk}.

T_k is determined by

$$\frac{dT_k}{dt} = -c_{vk}\left[\sum_{l\in\mathcal{H}^k} \tilde{a}_{kl}(V_{sk} - V_{sl}) + \tilde{g}_k(V_{sk} - V_{\mathrm{sref}})\right] \tag{21}$$

$$V_{\mathrm{sref}} = V_n + k_{\mathrm{PS}}(V_{\mathrm{cri}}^* - V_{\mathrm{cri}}) + k_{\mathrm{IS}}\int (V_{\mathrm{cri}}^* - V_{\mathrm{cri}})dt. \tag{22}$$

In (21), c_{vk} is a positive control gain. Equation (21) is a tracking problem, which results in V_{sk} of all MGs converging to V_{sref}. From (22), V_{sref} is obtained from a PI controller such that the system critical bus voltage V_{cri} can recover to its reference V_{cri}^*. k_{PS} and k_{IS} are the proportional and integral gains of the proportional and integral (PI) controller.

H_k is determined by

$$\frac{dH_k}{dt} = c_{Qk}\sum_{l\in\mathcal{H}^k} \tilde{a}_{kl}\,(\mathcal{Q}_{k,\mathrm{pin}} - \mathcal{Q}_{l,\mathrm{pin}}) \tag{23}$$

In (23), c_{Qk} is a positive control gain. Equation (23) is a synchronization problem, which results in $\mathcal{Q}_{k,\mathrm{pin}}$ of all MGs being equal with each other.

Finally, $V_{f\mathrm{ref}k}$ is obtained from a PI controller, which can make $V_{\mathrm{PCC}k}$ track its reference $V_{\mathrm{PCC}k}^*$, i.e.

$$V_{f\mathrm{ref}k} = V_{0\gamma} + k_{\mathrm{P}}(V_{\mathrm{PCC}k}^* - V_{\mathrm{PCC}k}) + k_{\mathrm{I}}\int (V_{\mathrm{PCC}k}^* - V_{\mathrm{PCC}k})dt \tag{24}$$

where k_{P} and k_{I} are, respectively, the proportional and integral gains of the PI controller, and $V_{0\gamma}$ is a voltage constant (normally set around rated voltage).

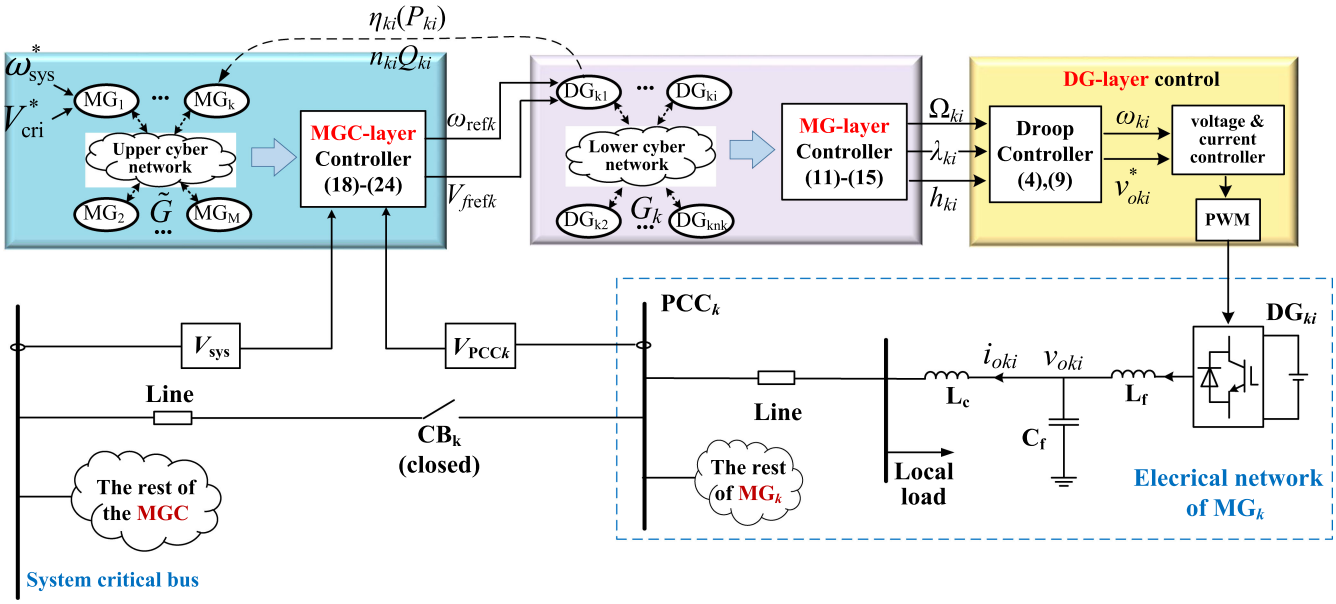

Fig. 2. Block diagram of the pinning-based hierarchical and distributed cooperative control for MGC.

Remark 3: For each MG, without loss of generality, the PCC voltage $V_{\mathrm{PCC}k}$ is selected to be controlled to its reference. One can also choose another node voltage in the MG to be controlled.

Remark 4: Since $\eta_{k,\mathrm{pin}}$ of all MGs are equal with each other, and the MG-layer control can ensure (8), it can be deduced that the GCIVs of all pinned DG units are equal and, furthermore, the GCIVs of all DG units in the MGC are equal. Therefore, an economic operation of the whole MGC system can be realized. Similarly, it can also be deduced that $n_{ki}Q_{ki}$ of all DG units in the MGC are equal, which results in an accurate reactive power sharing in the whole system.

D. Summary

Fig. 2 shows a block diagram of the proposed pinning-based hierarchical and distributed cooperative control for MGC. Note that for simplicity, only the most important control details are presented in Fig. 2. For the physical network, DG_{ki} is connected to the PCC bus of MG_k (PCC_k) through an *LCL* filter, local load bus, and feeder line. Then, MG_k is connected to the system critical bus and the rest of MGC through a circuit breaker (CB) (CB_k) and feeder line. The voltages of the system critical bus and PCC_k are measured and fed back to the MGC-layer controller. The general control implementation procedures in Fig. 2 are summarized in the following.

1) MGC-layer control: The system frequency and critical bus voltage reference ω^*_{sys} and V^*_{cri} are sent to the pinned MG agents. Then, the MGC-layer controllers in (18)–(24) are executed based on the information exchange among MG agents in the upper communication network $\widetilde{G}$. Finally, the frequency and voltage references $\omega_{\mathrm{ref}k}$ and $V_{f\mathrm{ref}k}$ for MG_k are obtained.
2) MG-layer control: $\omega_{\mathrm{ref}k}$ and $V_{f\mathrm{ref}k}$ are sent to the pinned DG units in MG_k. The pinned DG units also send their information of $\eta_{ki}(P_{ki})$ and $n_{ki}Q_{ki}$ to the corresponding MG agent. Then, the MG-layer controllers in (11)–(15) are executed based on the information exchange among DG units in the lower communication work G_k. Finally, the regulation variables Ω_{ki}, λ_{ki}, and h_{ki} are obtained.
3) DG-layer control: Ω_{ki}, λ_{ki}, and h_{ki} are sent to the droop controller in (4) and (9). Then, the output frequency and voltage references ω_{ki} and v^*_{oki} for DG_{ki} are obtained and, then, sent to the voltage and current controller. Finally, the pulsewidth modulation (PWM) signals are generated to control the inverter.

IV. Small-Signal Dynamic Modeling of MGC

This section presents the small-signal dynamic model of MGC system with the proposed pinning-based three-layer distributed cooperative control. A general modeling procedure in this section includes: 1) modeling individual DG unit; 2) combining DG unit models to obtain each individual MG model; 3) combining the models of all MGs; 4) modeling the MGC-layer controller; 5) considering the correlation between MG-layer and MGC-layer and, then, combining all the models to obtain the complete MGC system model. Detailed step-by-step modeling process and the details of parameter matrices are provided in Appendix B.

A. Individual MG Model

Without loss of generality, the local dq reference frame of DG_1 in MG_1, i.e., DG_{11}, is selected as the global common DQ-frame. Thus, we have $\omega_g = \omega_{11}$, where ω_g is the frequency of the global DQ-frame. Then, δ_{ki} is defined as the angle between the local dq-frame of DG_{ki} and the global DQ-frame, i.e.

$$\dot{\delta}_{ki} = \omega_{ki} - \omega_g. \tag{25}$$

This article mainly focuses on the dynamics of power droop controller, MG-layer controller, and MGC-layer controller,

while the fast dynamics of the voltage/current controllers and *LC* filters are not the focus of this article. Thus, they are omitted in the model by assuming

$$v_{odki} = v^*_{odki}, v_{oqki} = v^*_{oqki} \tag{26}$$

where v_{odki} and v_{oqki} are d-axis and q-axis components of the output voltage v_{oki} of DG_{ki}, as shown in Fig. 2.

Then, in light of (26), the small-signal dynamic model of DG_{ki} can be obtained by linearizing (11)–(15) and rearranging the linearized results, i.e.

$$\begin{aligned}\Delta\dot{X}_{\mathrm{inv}ki} = {} & A_{\mathrm{inv}ki}\Delta X_{\mathrm{inv}ki} + B_{\mathrm{inv}ki}\Delta i_{oDQki} + C_{\mathrm{inv}ki}\Delta\omega_g \\ & + \sum_{j\in\mathcal{N}_i^k} F_{\mathrm{inv}kij}\Delta X_{\mathrm{inv}kj} + H_{\mathrm{inv}ki}\Delta V_{f\mathrm{ref}k} \\ & + R_{\mathrm{inv}ki}\Delta\omega_{\mathrm{ref}k}\end{aligned} \tag{27}$$

where $A_{\mathrm{inv}ki}, B_{\mathrm{inv}ki}, C_{\mathrm{inv}ki}, F_{\mathrm{inv}kij}, H_{\mathrm{inv}ki}$, and $R_{\mathrm{inv}ki}$ are the parameter matrices and their details are provided in Appendix B. $F_{\mathrm{inv}kij}$ represents the correlations among DG units in MG_k due to their information exchange in the lower communication network. Δi_{oDQki} is the deviation of the DG_{ki} output current i_{oki}, as shown in Fig. 2, in the global DQ-frame. There are six state variables of DG_{ki}, given by

$$\Delta X_{\mathrm{inv}ki} = [\Delta\delta_{ki}, \Delta P_{ki}, \Delta Q_{ki}, \Delta\Omega_{ki}, \Delta\lambda_{ki}, \Delta h_{ki}]^T \tag{28}$$

where the superscript "T" represents the transpose of a matrix.

Combination of all the individual DG unit models in (28) in MG_k provides the small-signal dynamic model of MG_k, given by

$$\begin{aligned}\Delta\dot{X}_{\mathrm{INV}k} = {} & A_{\mathrm{INV}k}\Delta X_{\mathrm{INV}k} + B_{\mathrm{INV}k}\Delta i_{oDQk} + C_{\mathrm{INV}k}\Delta\omega_g \\ & + H_{\mathrm{INV}k}\Delta V_{f\mathrm{ref}k} + R_{\mathrm{INV}k}\Delta\omega_{\mathrm{ref}k}\end{aligned} \tag{29}$$

where $\Delta X_{\mathrm{INV}k} = [\Delta X^T_{\mathrm{inv}k1}, \Delta X^T_{\mathrm{inv}k2}, \ldots, \Delta X^T_{\mathrm{inv}kN_k}]^T$ and $\Delta i_{oDQk} = [\Delta i^T_{oDQk1}, \Delta i^T_{oDQk2}, \ldots, \Delta i^T_{oDQkN_k}]^T$. $A_{\mathrm{INV}k}$, $B_{\mathrm{INV}k}, C_{\mathrm{INV}k}, H_{\mathrm{INV}k}$, and $R_{\mathrm{INV}k}$ are parameter matrices.

In addition, by linearizing (13) and (26) and, then, combining the linearized results of all DG units in MG_k, we have

$$\Delta v_{oDQk} = L_{\mathrm{INV}k}\Delta X_{\mathrm{INV}k} \tag{30}$$

where Δv_{oDQk} is the deviation of v_{oki} of all the DG units in MG_k, and $L_{\mathrm{INV}k}$ is the parameter matrix.

B. Combination of All Individual MG's Models

By combining (30) of all the MGs, we have

$$\Delta v_{oDQ} = L_{\mathrm{INV}}\Delta X_{\mathrm{INV}} \tag{31}$$

where L_{INV} is the parameter matrix. Δv_{oDQ} is the combination of Δv_{oDQk} of all the MGs, i.e., $\Delta v_{oDQ} = [\Delta v^T_{oDQ1}, \Delta v^T_{oDQ2}, \ldots, \Delta v^T_{oDQM}]^T$. ΔX_{INV} is the combination of $\Delta X_{\mathrm{INV}k}$ of all the MGs, i.e., $\Delta X_{\mathrm{INV}} = [\Delta X^T_{\mathrm{INV}1}, \Delta X^T_{\mathrm{INV}2}, \ldots, \Delta X^T_{\mathrm{INV}M}]^T$.

For the network and load models, we consider the steady-state algebraic equations of the series *RL* lossy feeder lines and *RL*-type constant impedance loads. Therefore, their models are described by the node voltage equations $I = YU$ with Y being the node admittance matrix. The linearized form of $I = YU$ in this article is given by

$$\begin{bmatrix}\Delta i_{oDQ}\\ 0\end{bmatrix} = \underbrace{\begin{bmatrix}Y_A & Y_B\\ Y_C & Y_D\end{bmatrix}}_{:=Y_{aug}}\begin{bmatrix}\Delta v_{oDQ}\\ \Delta v_{NLDQ}\end{bmatrix} \tag{32}$$

where Y_{aug} can be obtained from Y, Δi_{oDQ} is the combination of Δi_{oDQk} of all the MGs, and Δv_{NLDQ} is the deviation of all the voltages of the network and load nodes. Note that, in (32), the injected currents corresponding to the network and load nodes are zero because the constant impedance type of loads is considered. A contractive form of (32) can be obtained by reducing the zero components of the injected currents, i.e.

$$\Delta i_{oDQ} = Y_M\Delta v_{oDQ} \tag{33}$$

where $Y_M = (Y_A - Y_B Y_D^{-1} Y_C)^{-1}$. Then, from (31) and (33), we have

$$\Delta i_{oDQ} = W_{\mathrm{INV}}\Delta X_{\mathrm{INV}},\ W_{\mathrm{INV}} = Y_M L_{\mathrm{INV}}. \tag{34}$$

To describe $V_{f\mathrm{ref}k}$ in (29), we focus on the linearized model of (24) in the following. Denote ψ_k as the state variable of (24), i.e.

$$\dot{\psi}_k = V^*_{\mathrm{PCC}k} - V_{\mathrm{PCC}k} \tag{35}$$

where $V_{\mathrm{PCC}k} = \sqrt{V^2_{\mathrm{PCC}Dk} + V^2_{\mathrm{PCC}Qk}}$. By linearizing (24) and (35), we have

$$\begin{aligned}\Delta V_{f\mathrm{ref}k} = {} & -k_{\mathrm{P}}A_{\mathrm{PCC}k}\Delta V_{\mathrm{PCC}DQk} + k_{\mathrm{I}}\Delta\psi_k \\ & + k_{\mathrm{P}}\Delta V^*_{\mathrm{PCC}k},\end{aligned} \tag{36}$$

$$\Delta\dot{\psi}_k = -A_{\mathrm{PCC}k}\Delta V_{\mathrm{PCC}DQk} + \Delta V^*_{\mathrm{PCC}k} \tag{37}$$

where $\Delta V_{\mathrm{PCC}DQk} = [\Delta V_{\mathrm{PCC}Dk}, \Delta V_{\mathrm{PCC}Qk}]^T$, and $A_{\mathrm{PCC}k}$ is the parameter matrix. Since $\Delta V_{\mathrm{PCC}DQk}$ is part of Δv_{NLDQ}, based on (32), it can be expressed in terms of Δi_{oDQ} as

$$\Delta V_{\mathrm{PCC}DQk} = Z_{\mathrm{PCC}k}\Delta i_{oDQ} \tag{38}$$

where $Z_{\mathrm{PCC}k}$ can be obtained from Y_{aug}.

To describe $\Delta\omega_g$ in (29), we linearize (11) for DG_{11}. Thus, $\Delta\omega_g$ can be expressed as

$$\Delta\omega_g = D_{\mathrm{INV}}\Delta X_{\mathrm{INV}} \tag{39}$$

where D_{INV} is the parameter matrix.

Then, the combination model of all the individual MGs can be formulated by substituting (36), (38), (39) into the individual MG model (29), combining the models of all the individual MGs, and substituting (34) into the combined results, i.e.

$$\begin{aligned}\Delta\dot{X}_{\mathrm{INV}} = {} & J_{\mathrm{INV}}\Delta X_{\mathrm{INV}} + k_{\mathrm{I}}H_{\mathrm{INV}}\Delta\overline{\psi} \\ & + k_{\mathrm{P}}H_{\mathrm{INV}}\Delta V^*_{\mathrm{PCC}} + R_{\mathrm{INV}}\Delta\omega_{\mathrm{ref}}\end{aligned} \tag{40}$$

where

$$\begin{aligned}J_{\mathrm{INV}} = {} & A_{\mathrm{INV}} + C_{\mathrm{INV}}D_{\mathrm{INV}} + B_{\mathrm{INV}}W_{\mathrm{INV}} \\ & - k_{\mathrm{P}}N_{\mathrm{INV}}W_{\mathrm{INV}}.\end{aligned} \tag{41}$$

In (40) and (41), $A_{\rm INV}, B_{\rm INV}, C_{\rm INV}, H_{\rm INV}, R_{\rm INV}$, and $N_{\rm INV}$ are parameter matrices, $\Delta\overline{\psi} = [\Delta\psi_1, \Delta\psi_2, \ldots, \Delta\psi_M]^T$, $\Delta V^*_{\rm PCC} = [\Delta V^*_{\rm PCC1}, \Delta V^*_{\rm PCC2}, \ldots, \Delta V^*_{{\rm PCC}M}]^T$, and $\Delta\omega_{\rm ref} = [\Delta\omega_{\rm ref1}, \Delta\omega_{\rm ref2}, \ldots, \Delta\omega_{{\rm ref}M}]^T$.

In addition, the state-space equation of $\Delta\overline{\psi}$ can be formulated by substituting (38) into (37), combining the substituted results of all MGs, and substituting (34) into the combined results, i.e.

$$\Delta\dot{\overline{\psi}} = -T_{\rm PCC}W_{\rm INV}\Delta X_{\rm INV} + \Delta V^*_{\rm PCC} \tag{42}$$

where $T_{\rm PCC}$ is the parameter matrix.

C. Modeling of MGC-Layer Controller

From (20), we have

$$V_{sk} = V_{0\beta} + T_k. \tag{43}$$

For the MGC-layer controller of $\rm MG_{\it k}$ agent, linearizing (18), (19), (21), (23), and (43) and rearranging the linearized results yield

$$\Delta\dot{S}_{{\rm MG}k} = A_{{\rm MGC}k}\Delta S_{{\rm MG}k} + \sum_{l\in\mathcal{H}^k} F_{{\rm MGC}kl}\Delta S_{{\rm MG}l} + H_{{\rm MGC}k}\Delta V_{\rm sref} + E_{{\rm MGC}k}\Delta X_{\rm INV} \tag{44}$$

where $\Delta S_{{\rm MG}k} = [\Delta\Phi_k, \Delta T_k, \Delta H_k]^T$, $A_{{\rm MGC}k}$, $F_{{\rm MGC}kl}$, $H_{{\rm MGC}k}$, and $E_{{\rm MGC}k}$ are parameter matrices. $F_{{\rm MGC}kl}$ represents the correlations among MG agents due to their information exchange in the upper communication network. $E_{{\rm MGC}k}$ represents the correlations from pinned DG units to MG agents by the pinning links.

By combining (44) of all the MG agents, we have

$$\Delta\dot{S}_{\rm MG} = A_{\rm MGC}\Delta S_{\rm MG} + H_{\rm MGC}\Delta V_{\rm sref} + E_{\rm MGC}\Delta X_{\rm INV} \tag{45}$$

where $\Delta S_{\rm MG} = [\Delta S^T_{\rm MG1}, \Delta S^T_{\rm MG2}, \ldots, \Delta S^T_{{\rm MG}M}]^T$, $A_{\rm MGC}$, $H_{\rm MGC}$, and $E_{\rm MGC}$ are parameter matrices.

To describe $\Delta V_{\rm sref}$ in (45), we focus on the linearized model of (22) in the following. Denote φ as the state variable of (22), i.e.

$$\dot{\varphi} = V^*_{\rm cri} - V_{\rm cri} \tag{46}$$

where $V_{\rm cri} = \sqrt{V^2_{{\rm cri}D} + V^2_{{\rm cri}Q}}$. By linearizing (22) and (46), we have

$$\Delta V_{\rm sref} = -k_{\rm PS}A_{\rm cri}\Delta V_{{\rm cri}DQ} + k_{\rm IS}\Delta\varphi \tag{47}$$

$$\Delta\dot{\varphi} = -A_{\rm cri}\Delta V_{{\rm cri}DQ} \tag{48}$$

where $\Delta V_{{\rm cri}DQ} = [\Delta V_{{\rm cri}D}, \Delta V_{{\rm cri}Q}]^T$, and $A_{\rm cri}$ is the parameter matrix. Since $\Delta V_{{\rm cri}DQ}$ is part of Δv_{NLDQ}, based on (32), it can be expressed as

$$\Delta V_{{\rm cri}DQ} = Z_{\rm cri}\Delta i_{oDQ} \tag{49}$$

where $Z_{\rm cri}$ can be obtained from Y_{aug}.

Then, substituting (34), (47), and (49) into (45) yields

$$\Delta\dot{S}_{\rm MG} = A_{\rm MGC}\Delta S_{\rm MG} + J_{\rm MGC}\Delta X_{\rm INV} + k_{\rm IS}H_{\rm MGC}\Delta\varphi \tag{50}$$

where

$$J_{\rm MGC} = E_{\rm MGC} - k_{\rm PS}H_{\rm MGC}A_{\rm cri}Z_{\rm cri}W_{\rm INV}. \tag{51}$$

Moreover, substituting (34) and (49) into (48) yields

$$\Delta\dot{\varphi} = -A_{\rm cri}Z_{\rm cri}W_{\rm INV}\Delta X_{\rm INV}. \tag{52}$$

D. Complete MGC System Model

To further formulate the models of (40) and (42), we need to express $\Delta V^*_{\rm PCC}$ and $\Delta\omega_{\rm ref}$ in terms of $\Delta S_{\rm MG}$, which can be done by linearizing (18) and (20) and, then, combining the linearized results of all MGs, given by

$$\Delta\omega_{\rm ref} = A_{\rm cou}\Delta S_{\rm MG} \tag{53}$$

$$\Delta V^*_{\rm PCC} = B_{\rm cou}\Delta S_{\rm MG} \tag{54}$$

where $A_{\rm cou}$ and $B_{\rm cou}$ are parameter matrices.

Finally, the complete MGC system model can be formulated by substituting (53) and (54) into (40) and (42), and combining the substituted results and (50) and (52), i.e.

$$\Delta\dot{X}_{\rm sys} = A_{\rm sys}\Delta X_{\rm sys} \tag{55}$$

where $\Delta X_{\rm sys} = [\Delta X^T_{\rm INV}, \Delta\overline{\psi}^T, \Delta S^T_{\rm MG}, \Delta\varphi]^T$, and $A_{\rm sys}$ is the state matrix of the MGC system.

The system small-signal stability can be evaluated based on analyzing the eigenvalues and eigen-structure of $A_{\rm sys}$, which will be presented in Section V-B.

V. Numerical Study

Based on a test MGC system, this section provides the system stability analysis (see Section V-B) and time-domain simulation results in the PSCAD/EMTDC platform (see Section V-C) to validate the effectiveness of the proposed methods.

A. Study System

Fig. 3 shows a schematic diagram of the studied 23-bus three-phase MGC system, which is a 0.38 kV and 50 Hz system including three MGs, 9 DG units, 12 feeder lines, and 11 loads. The MGC is connected to the utility grid through a CB and 10 kV/0.38 kV transformer. The CB is open, i.e, the system is operated in the islanded mode. $\rm CB_1$–$\rm CB_3$ are the CBs of each MG. They are closed. Bus 23 is the system critical bus, which is the common bus connecting to all MGs. Buses 19, 20, and 21 are the PCC bus of each MG. Each feeder line is modeled by a series *RL* branch and each load is represented by a series *RL* impedance. L_c is the coupling inductance. The system electrical parameters are shown in Table I.

Fig. 4 shows the upper and lower communication networks of the studied MGC system, where the arrowed and dotted lines denote the communication links. $\rm MG_1$ is the pinned MG agent, which receives the references of $\omega^*_{\rm sys}$ and $V^*_{\rm cri}$. $\rm DG_{11}$, $\rm DG_{21}$, and $\rm DG_{31}$ are the pinned DG units of each MG. The corresponding associated adjacency matrix and leader-adjacency matrix parameters are provided in Appendix A.

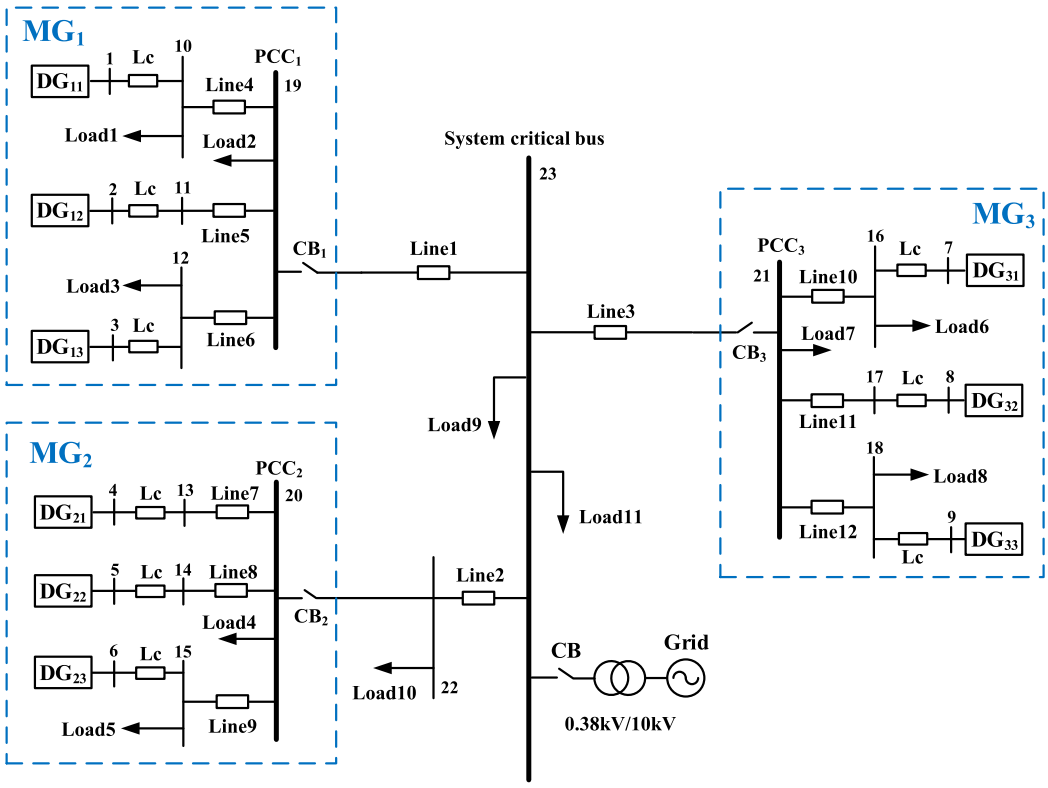

Fig. 3. Schematic diagram of the studied MGC system.

TABLE I
ELECTRICAL PARAMETERS OF THE MGC SYSTEM

Type	Electrical parameters
Line	Line1=0.008Ω+0.03mH, Line2=0.005Ω+0.02mH, Line3=0.014Ω+0.07mH, Line4,8,10,11=0.15Ω+0.15mH, Line5,9=0.11Ω+0.35mH, Line6,7,12=0.11Ω+0.2mH
Load	Load1,5,8=15kW+7.5kVar, Load2=40kW+15kVar, Load3,6=12kW+5kVar, Load4,7=50kW+20kVar, Load9=75kW+22.5kVar, Load10=2kW+5kVar, Load11=20kW+10kVar

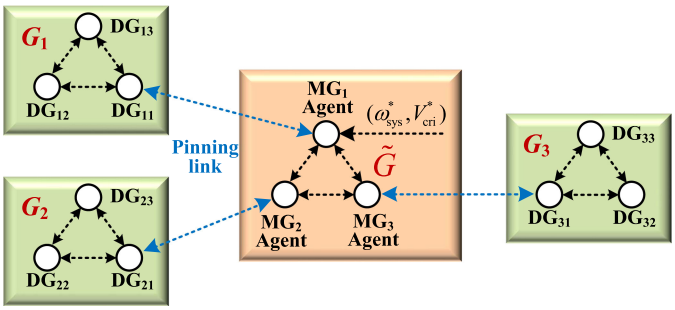

Fig. 4. Double-layer distributed communication network of the studied MGC system.

The generation cost function $\mathrm{GC}_{ki}(P_{ki})$ in this article is described by the quadratic function [31], i.e.

$$\mathrm{GC}_{ki}(P_{ki}) = \alpha_{ki} P_{ki}^2 + \beta_{ki} P_{ki} + \gamma_{ki} \tag{56}$$

TABLE II
GENERATION COST PARAMETERS

	α_{ki}	β_{ki}	γ_{ki}
$\mathrm{DG}_{11}\mathrm{DG}_{12}\mathrm{DG}_{13}$ (MG_1)	0.094	1.22	51
$\mathrm{DG}_{21}\mathrm{DG}_{22}\mathrm{DG}_{23}$ (MG_2)	0.078	3.41	31
$\mathrm{DG}_{31}\mathrm{DG}_{32}\mathrm{DG}_{33}$ (MG_3)	0.105	2.53	78

TABLE III
PARAMETERS OF DG-LAYER CONTROL

Parameters	k_{ed}	n_{ki} (kV/kVar$\times 10^{-3}$)	$P_{\max}$ (kW)	$Q_{\max}$ (kVar)
$\mathrm{DG}_{11}\mathrm{DG}_{12}\mathrm{DG}_{13}$	0.1	0.78	60	20
$\mathrm{DG}_{21}\mathrm{DG}_{22}\mathrm{DG}_{23}$	0.1	0.52	50	30
$\mathrm{DG}_{31}\mathrm{DG}_{32}\mathrm{DG}_{33}$	0.1	0.78	60	20

where α_{ki}, β_{ki}, and γ_{ki} are cost parameters. Table II shows the cost parameters of each DG unit [31].

Tables III and IV provide the parameters of the DG-layer, MG-layer, and MGC-layer controls, where $P_{\max}$ and $Q_{\max}$ are the active/reactive power capacities of DG units.

B. Eigen-Analysis Results

1) Eigenvalue Spectrum: Fig. 5 compares the low-frequency eigenvalue spectrum of the MGC system with and without the MGC-layer control in service. In Case 1 (cyan squares), there are only DG and MG-layer controls for the MGC system. In Case 2

TABLE IV
PARAMETERS OF MG-LAYER AND MGC-LAYER CONTROL

Parameters	MG-layer	MGC-layer
$c_{\omega ki}/c_{\omega k}$	560	200
c_{Pki}/c_{Pk}	95	35
c_{vki}/c_{vk}	20	5
c_{Qki}/c_{Qk}	60	13
k_{P}	/	25
k_{I}	/	200
k_{PS}	/	5
k_{IS}	/	67

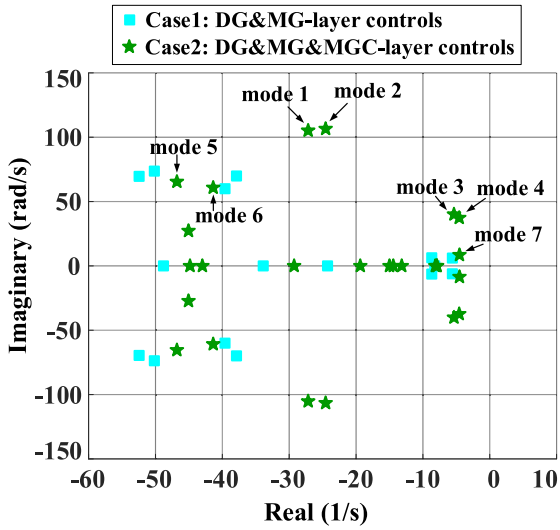

Fig. 5. Low-frequency eigenvalue spectrum of the studied MGC system with and without the MGC-layer control.

TABLE V
DOMINANT OSCILLATORY MODES WITH MGC-LAYER CONTROL

	eigenvalue	damping
mode 1	-27.17±j105.20	0.250
mode 2	-24.42±j106.51	0.223
mode 3	-5.33±j40.08	0.132
mode 4	-4.57±j37.45	0.121
mode 5	-46.80±j65.43	0.582
mode 6	-41.37±j60.82	0.562
mode 7	-4.53±j8.51	0.470

(green stars), the MGC-layer control is added. Fig. 5 indicates that the MGC-layer control 1) significantly changes the shaping of eigenvalues on the complex plane, and 2) introduces some new oscillation modes to the system. The dominant oscillation modes of Case 2 are labeled as modes 1–7 in Fig. 5. Table V shows their corresponding eigenvalues and dampings. The frequency range of modes 1–7 varies from 8.51 to 106.55 rad/s, which indicates a "wide-frequency-band oscillation." In addition, modes 1–4 are with relatively low dampings, which may lead to more oscillatory responses compared with Case 1.

2) Participation Factor Analysis: Participation factor is the multiplication of the corresponding element in the right and left eigenvectors of the state matrix. It can be used for evaluating the association degree between state variables and modes. In this article, we perform the participation factor analysis based on the state matrix A_{sys} in (55).

Fig. 6 shows the participation factor analysis results for modes 1, 3, 5, and 7. Note that the results of modes 2, 4, and 6 are similar to those of modes 1, 3, and 5 and, thus, not presented for simplicity. The variables in the horizontal axis of Fig. 6 correspond to the state variables. States $\Delta\delta_{ki}, \Delta P_{ki}, \Delta Q_{ki}, \Delta\Omega_{ki}, \Delta\lambda_{ki}, \Delta h_{ki}$, which belong to DG units (DG_{11}–DG_{33}), mainly correspond to the DG-layer and MG-layer controls. States $\Delta\psi_k, \Delta\Phi_k, \Delta T_k, \Delta H_k$, which belong to MG agents (MG_1–MG_3), and $\Delta\varphi$ mainly correspond to the MGC-layer control. The vertical axis shows the participation factor value. A higher value indicates a stronger association between the state variable and the analyzed mode. Moreover, to better understand Fig. 6, we take $\Delta\delta_{ki}$ as an example. For the position of $\Delta\delta_{ki}$ in Fig. 6, the participation factor values of $\Delta\delta_{ki}$ of different DG units are stacked together.

The results of Fig. 6 are summarized as follows.

1) Modes 1 and 3 are "interaction modes" because the state variables of both DG and MG-layer and MGC-layer contribute to modes 1 and 3. From Table V, modes 1 and 3 are with relatively low dampings. Therefore, it can be deduced that the control layer interaction may result in low-damping modes.
2) Mode 5 is a kind of "DG and MG-layer mode" since the state variables of DG and MG-layer mainly contribute to it.
3) Mode 7 is a kind of "MGC-layer mode" since the state variables of MGC-layer mainly contribute to it. From Table V, the oscillation frequency of mode 7 is the lowest. This is because the response speed of the MGC-layer control should be slow enough to ensure a time-scale separation between MGC-layer and MG-layer.
4) States $\Delta Q_{ki}, \Delta h_{ki}$, and ΔH_k, which are associated with the reactive power controllers (15) and (23), are generally the states with the highest contribution to modes 1, 3, 5, and 7. Therefore, controllers (15) and (23) are the key controllers, which affect the system dynamics most significantly.

3) Sensitivity Analysis–Impact of MGC-Layer Control Parameters on System Stability: Fig. 7 shows the traces of the dominant oscillatory modes 1–7 as a function of the MGC-layer control parameters $c_{\omega k}, c_{Pk}, c_{vk}$, and c_{Qk}, where the blue circles denote eigenvalues with beginning parameters, and purple diamonds denote eigenvalues with ending parameters. Corresponding to Fig. 7, Table VI summarizes the variation trends of the mainly affected modes when increasing the MGC-layer control parameters. Note that the results of increasing k_{P} and k_{PS} are shown in Table VI while not in Fig. 7 for simplicity, and parameters k_{I} and k_{IS} have little impact on modes 1–7 and, thus, their results are not presented. Fig. 7 and Table VI indicate the following.

1) The system may lose stability with variations of control parameters, i.e., there are eigenvalues located in the right half plane with improper parameters. Therefore, the

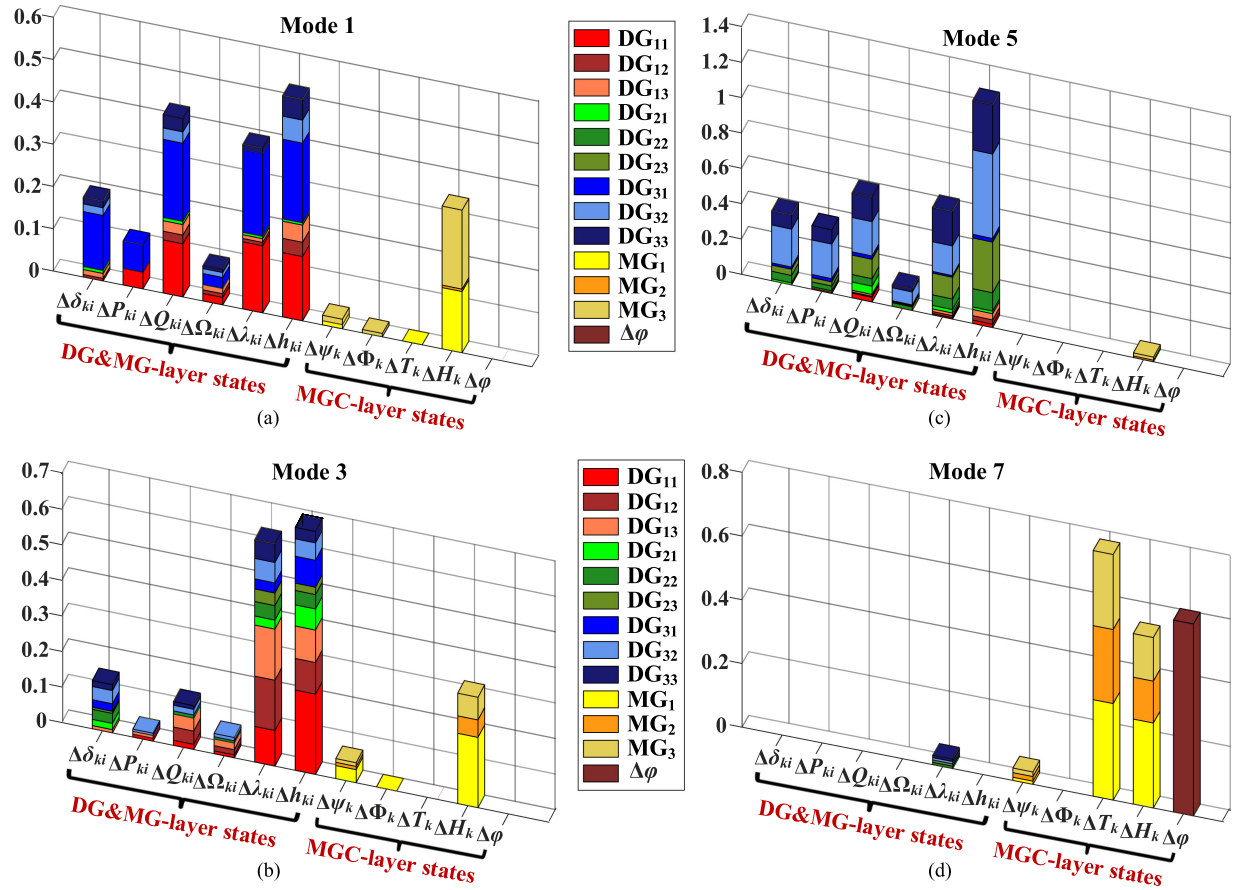

Fig. 6. Participation factors of (a) mode 1, (b) mode 3, (c) mode 5, and (d) mode 7, which describe the association degrees between state variables and modes. The variables in the horizontal axis correspond to the state variables. States $\Delta\delta_{ki}, \Delta P_{ki}, \Delta Q_{ki}, \Delta\Omega_{ki}, \Delta\lambda_{ki}, \Delta h_{ki}$, which belong to DG units (DG_{11}–DG_{33}), mainly correspond to the DG-layer and MG-layer controls. States $\Delta\psi_k, \Delta\Phi_k, \Delta T_k, \Delta H_k$, which belong to MG agents (MG_1–MG_3), and $\Delta\varphi$ mainly correspond to the MGC-layer control. The vertical axis shows the participation factor value.

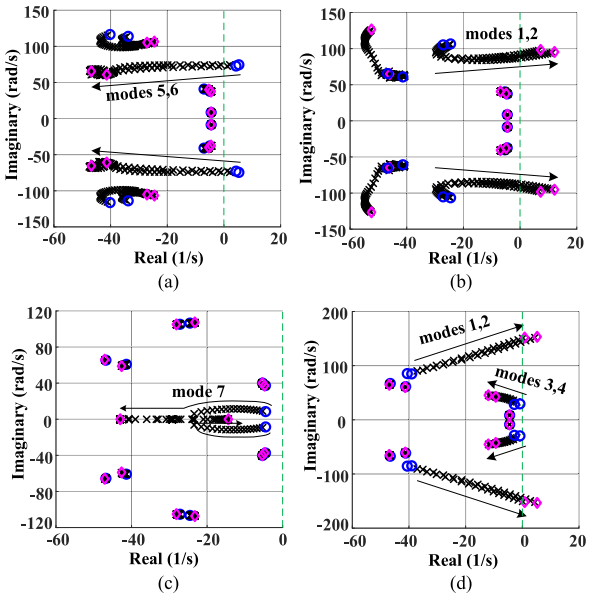

Fig. 7. Traces of dominant oscillatory modes when (a) $c_{\omega k}$ varies from 30 to 200, (b) c_{Pk} varies from 35 to 300, (c) c_{vk} varies from 5 to 40, and (d) c_{Qk} varies from 5 to 40. Blue circles denote eigenvalues with beginning parameters, and purple diamonds denote eigenvalues with ending parameters.

TABLE VI
VARIATION TRENDS OF DOMINANT OSCILLATORY MODES WHEN INCREASING MGC-LAYER CONTROL PARAMETERS

Parameter	Mainly affected modes	Modes variation when increasing parameters
$c_{\omega k}$	modes 5,6	move towards stable region
c_{Pk}	modes 1,2	move towards unstable region
c_{vk}	mode 7	move towards stable region first, then splits at the real axis
c_{Qk}	modes 1,2	move towards unstable region
	modes 3,4	move towards stable region
k_{PS}	mode 7	move towards stable region
k_{P}	modes 1,2	move towards unstable region
	modes 3,4	move towards stable region

control parameters should be carefully selected to ensure sufficient stability.

2) The system dynamics are relatively complex. One parameter may affect different modes, and one mode may be affected by different parameters, e.g., modes 1 and 2 are affected by c_{Pk}, c_{Qk}, and k_{P}.

3) In particular, Fig. 7(d) indicates that increasing c_{Qk} has an opposite effect on the variation trends of modes 1, 2 and modes 3, 4. Therefore, the selection of c_{Qk} should consider a tradeoff between the dynamic performance of modes 1, 2 and modes 3, 4. In addition, c_{Qk} is the control parameter of controller (23), which is a key controller from the previous analysis. Hence, the selection of c_{Qk} is of vital importance.

In sum, the system dynamics is relatively complicated due to multiple control layers and control parameters. The above analysis can facilitate a better understanding of the system dynamics and stability characteristics, and also provide a general guideline for the control parameter tuning. The control parameter selection can also be formulated as an optimization problem to achieve largest stability margin and best dynamic performance by optimizing control parameters. This research will be included in our future work.

C. Time-Domain Simulation Results

The MGC system is initially operated with the DG-layer control. At t = 8 s, the MG-layer control is activated. At t = 17 s, the MGC-layer control is employed. Fig. 8 shows the corresponding simulation results.

1) Fig. 8(a) indicates that the DG-layer control results in a frequency deviation, while the system frequency is restored to the rated value 50 Hz after applying the MG-layer control. This is because in our study, $\omega_{\mathrm{ref}k}$ of each MG is set to be the rated frequency by default if without MGC-layer control. After the MGC-layer control is employed at t = 17 s, $\omega_{\mathrm{ref}k}$ is regulated by (18) and (19), and the system frequency is maintained at 50 Hz.
2) Fig. 8(b) indicates that the system critical bus voltage exhibits deviations during the DG-layer and MG-layer controls, while it can be restored to the rated value 1 p.u. by the MGC-layer controller.
3) Fig. 8(c) indicates that during the stage of DG-layer control, the GCIVs (η_{ki}) of all DG units are equal due to the regulating characteristic of droop equation in (9). After the MG-layer control is activated, the neighbor communications in the lower communication networks result in a consensus of GCIVs for each individual MG, while the consensus values for different MGs could be different. After the MGC-layer control is employed, it can realize a coordination among different MGs with the help of pinning links and the upper communication network, and, thus, the GCIVs of all DG units become equal again, indicating an economic operation of the whole system.
4) Fig. 8(d) indicates that under the DG-layer control the reactive power sharing is not accurate. After t = 8 s, the MG-layer control can impose an accurate reactive power sharing inside each individual MG. After t = 17 s, an accurate reactive power sharing for the whole MGC system is realized by the MGC-layer control. Note that the reactive power is shared based on n_{ki} shown in Table III.

In sum, the control objectives can be well realized with the proposed pinning-based hierarchical and distributed cooperative control method.

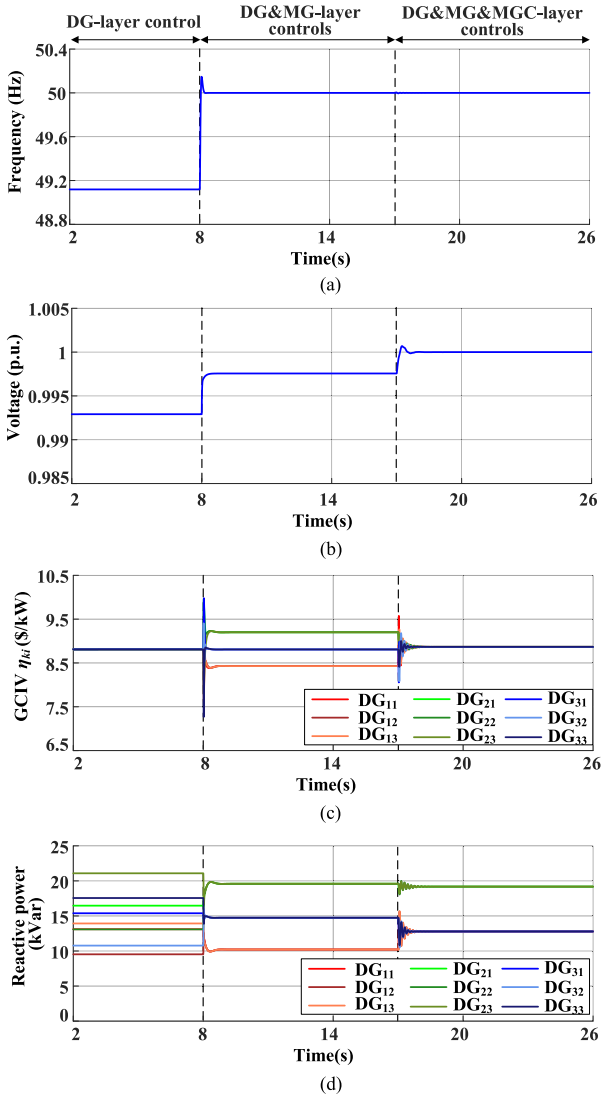

Fig. 8. Simulation results of (a) system frequency, (b) system critical bus voltage V_{cri}, (c) DG GCIV η_{ki}, and (d) DG output reactive powers Q_{ki}. The system is initially operated with the DG-layer control. At t = 8 s, the MG-layer control is activated, and at t = 17 s, the MGC-layer control is employed.

VI. Experimental Results

This section presents experimental results to validate the practical implementation feasibility of the proposed control method. Three experimental studies are carried out. Study 1 validates the basic control performance. Studies 2 and 3 evaluate the control performance under conditions of load changes and communication link failures, respectively.

A. Experimental Setup

Fig. 9 shows the hardware setup for the experimental MGC system in the laboratory. The experimental setup includes a dSPACE DS1006 platform, four Danfoss inverters, *RL* branch lines, resistive and inductive loads, switches to control the relays, and a control desk. The voltage and current are measured through LEM measurement boards and, then, processed by ADC boards. The signals after ADC boards are fed back to the dSPACE DS1006 platform, in which the control strategy is programmed

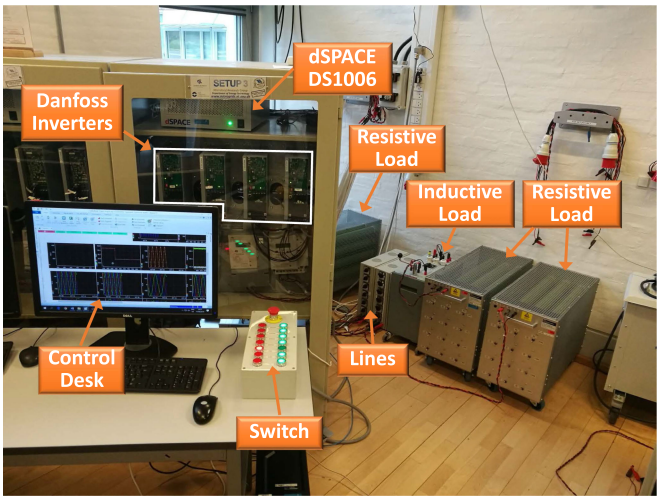

Fig. 9. Experimental setup in the laboratory.

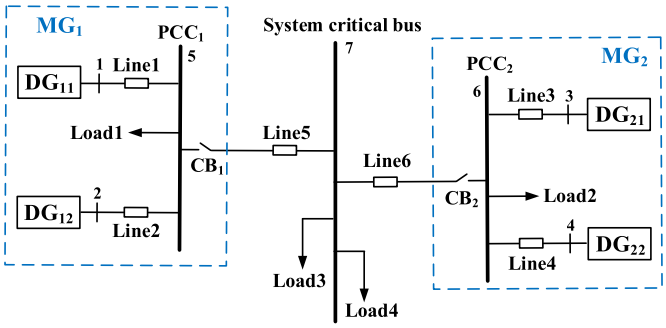

Fig. 10. Physical configuration of the experimental MGC system.

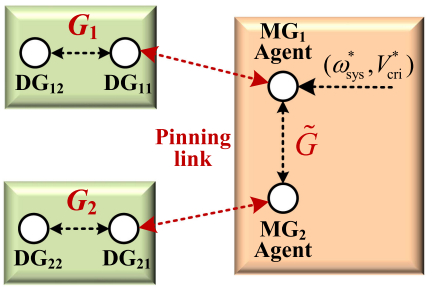

Fig. 11. Topology of the double-layer distributed communication network for the experimental MGC system.

and, then, executed in real time. Finally, the dSPACE generates PWM signals to switch the inverters with a switching frequency of 10 kHz. The control desk installed in a PC is responsible for monitoring the system states and measurements. The communication between dSPACE and PC is based on Ethernet cables.

Fig. 10 shows the physical configuration of the experimental MGC system, which includes 2 MGs, 4 DG units, 6 feeder lines, and 4 loads. The system rated frequency is 50 Hz and rated line-to-line RMS voltage is 215 V. The CBs CB_1 and CB_2 are closed. Bus 7 is the system critical bus. Buses 5 and 6 are the PCC buses for MG_1 and MG_2. Fig. 11 shows the double-layer distributed communication network for the experimental MGC system. In the upper cyber network $\widetilde{G}$, MG_1 agent receives the references ω^*_{sys} and V^*_{cri}. In the lower cyber networks G_1 and G_2, DG_{11} and DG_{21} are the pinned DG units of MG_1 and MG_2, respectively.

The system electrical parameters, generation cost parameters, DG-layer, MG-layer, and MGC-layer control parameters are shown in Tables VII–Table X. The ratio of reactive power capacities among DG units is $Q_{\mathrm{max11}} : Q_{\mathrm{max12}} : Q_{\mathrm{max21}} : Q_{\mathrm{max22}} = 4 : 3 : 4 : 3$.

TABLE VII
ELECTRICAL PARAMETERS OF EXPERIMENTAL MGC SYSTEM

Type	Electrical parameters
Inverter	Filter inductance: 1.8mH Filter capacitance: $27\mu F$
Line	Line1=1.8mH, Line2=1.8mH Line3=1.8mH, Line4=1.8mH Line5=1.9Ω+2.5mH, Line6=1.6Ω+2.1mH
Load	Load1=92Ω, Load2=153.3Ω, Load3=39.8Ω+j32.6Ω, Load4=120.2Ω+j37.1Ω

TABLE VIII
GENERATION COST PARAMETERS FOR EXPERIMENTAL MGC SYSTEM

	α_{ki}	β_{ki}	γ_{ki}
DG_{11}	0.108	0.23	0.7
DG_{12}	0.127	0.15	0.9
DG_{21}	0.108	0.23	0.7
DG_{22}	0.127	0.15	0.9

TABLE IX
PARAMETERS OF DG-LAYER CONTROL FOR EXPERIMENTAL MGC SYSTEM

Parameters	k_{ed}	n_{ki} (V/Var$\times 10^{-3}$)	$P_{\max}$ (kW)	$Q_{\max}$ (kVar)
DG_{11}	2	6.479	1.8	1.2
DG_{12}	2	8.639	1.35	0.9
DG_{21}	2	6.479	1.8	1.2
DG_{22}	2	8.639	1.35	0.9

TABLE X
PARAMETERS OF MG-LAYER AND MGC-LAYER CONTROLS FOR EXPERIMENTAL MGC SYSTEM

Parameters	MG-layer	MGC-layer
$c_{\omega ki}/c_{\omega k}$	400	80
c_{Pki}/c_{Pk}	400	80
c_{vki}/c_{vk}	150	30
c_{Qki}/c_{Qk}	20	2
k_{P}	/	1.2
k_{I}	/	42
k_{PS}	/	0.3
k_{IS}	/	10

B. Study 1: Basic Control Performance Validation

The DG-layer control is engaged initially. At $\mathrm{t} = \mathrm{t}_1$, the MG-layer control is activated, and at $\mathrm{t} = \mathrm{t}_2$, the MGC-layer control is introduced. Fig. 12 shows the corresponding experimental results. Fig. 12(a) indicates that the system frequency

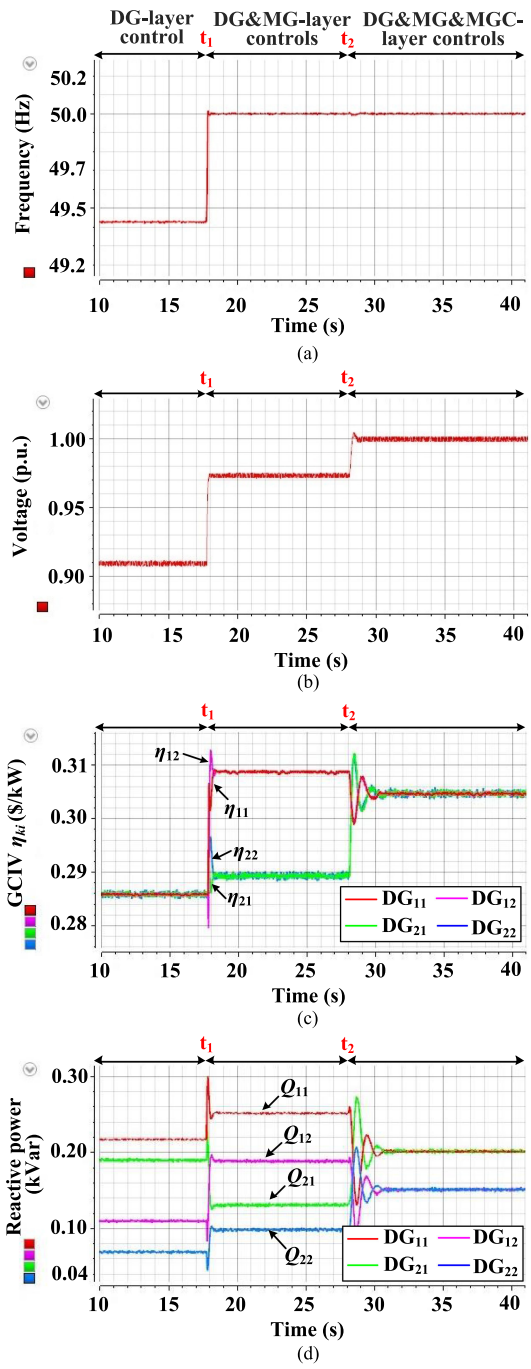

Fig. 12. Experimental results for Study 1—basic control performance evaluation: (a) system frequency, (b) system critical bus voltage, (c) DG GCIV η_{ki}, and (d) DG output reactive powers Q_{ki}. The DG-layer control is engaged initially. At $t = t_1$, the MG-layer control is activated, and at $t = t_2$, the MGC-layer control is introduced.

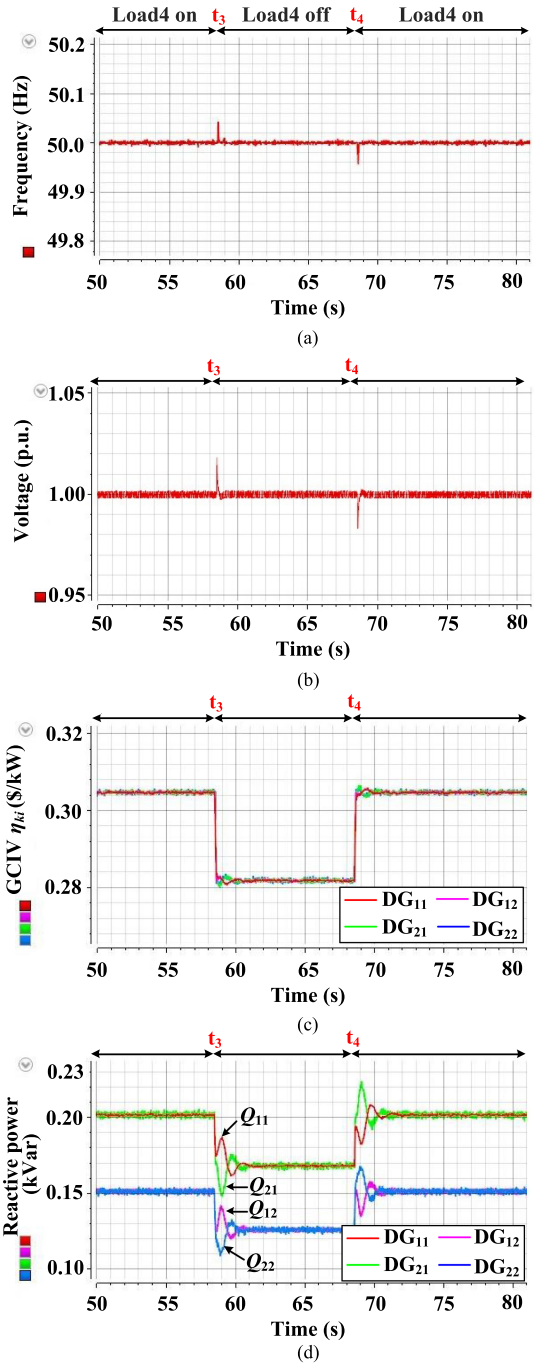

Fig. 13. Experimental results for Study 2—load change performance evaluation: (a) system frequency, (b) system critical bus voltage, (c) DG GCIV η_{ki}, and (d) DG output reactive powers Q_{ki}. The system is operated under the three-layer controls. At $t = t_3$, Load 4 is switched OFF. At $t = t_4$, Load 4 is switched ON again.

can be restored and, then, maintained at the rated value 50 Hz by the MG-layer and MGC-layer controls after $t = t_1$. Fig. 12(b) indicates that the MGC-layer control can restore the system critical bus voltage to the rated value 1 p.u. after $t = t_2$. Fig. 12(c) indicates that the GCIVs (η_{ki}) of all DG units are equal at the stage of DG layer control, after $t = t_1$, η_{ki} inside each individual MG are equal, i.e., $\eta_{11} = \eta_{12}$ and $\eta_{21} = \eta_{22}$, due to the regulating effect of MG-layer control, and after $t = t_2$, the MGC-layer control imposes equal η_{ki} of all DG units again, realizing a minimum generation cost of the whole system. Fig. 12(d) indicates that the reactive power sharing is not accurate before $t = t_1$, an accurate reactive power sharing inside each individual MG, i.e., $Q_{11} : Q_{12} = 4 : 3$ and $Q_{21} : Q_{22} = 4 : 3$, is realized after applying the MG-layer control, and after $t = t_2$, the MGC-layer control can achieve an accurate reactive power sharing across the whole system, i.e., $Q_{11} : Q_{12} : Q_{21} : Q_{22} = 4 : 3 : 4 : 3$.

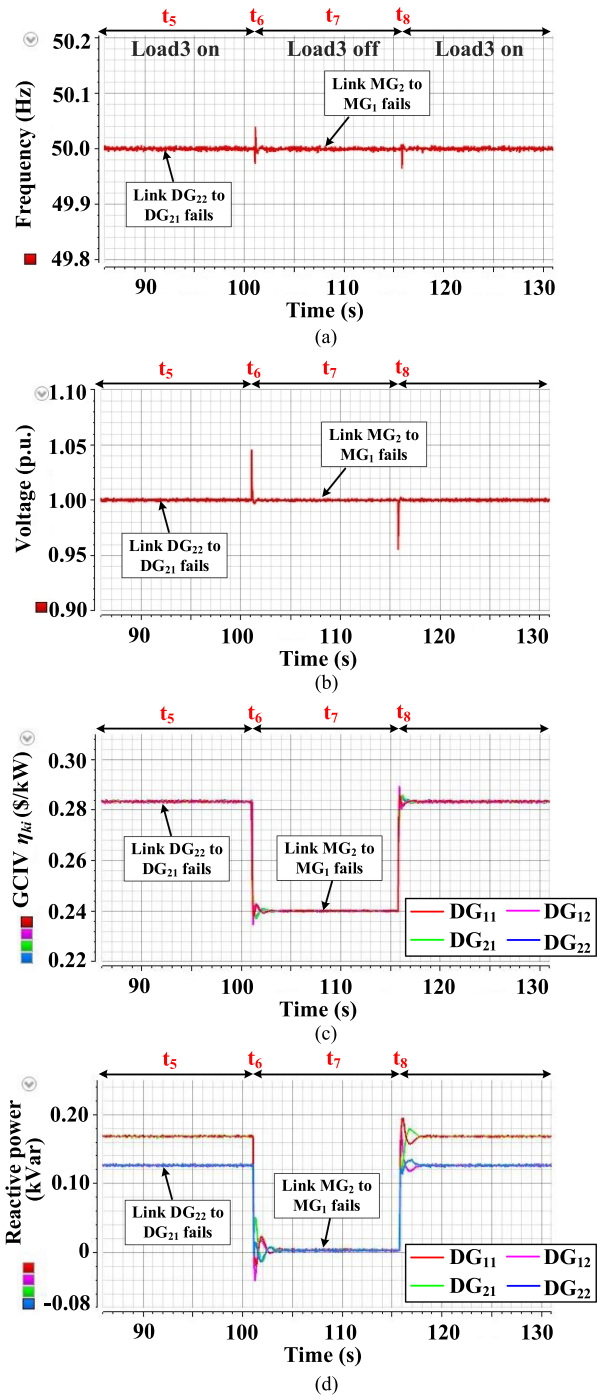

Fig. 14. Experimental results for Study 3—communication link failure resiliency: (a) system frequency; (b) system critical bus voltage; (c) DG GCIV η_{ki}; and (d) DG output reactive powers Q_{ki}. The system is operated under the three-layer controls. At $t = t_5$, the communication link from DG_{22} to DG_{21} fails. At $t = t_6$, Load 3 is switched OFF. At $t = t_7$, the communication link from MG_2 agent to MG_1 agent fails. At $t = t_8$, Load 3 is switched ON again.

C. Study 2: Load Change Performance Evaluation

The system is operated under the three-layer controls. At $t = t_3$, Load 4 is switched OFF. At $t = t_4$, Load 4 is switched ON again. Fig. 13 indicates that after Load 4 switched OFF and switched ON, the proposed three-layer control can always maintain the system frequency at 50 Hz, as shown in Fig. 13(a), maintain the system critical bus voltage at 1 p.u., as shown in Fig. 13(b), impose equal η_{ki} of all DG units, as shown in Fig. 13(c), and realize an accurate reactive power sharing $Q_{11} : Q_{12} : Q_{21} : Q_{22} = 4 : 3 : 4 : 3$ across the whole system, as shown in Fig. 13(d).

D. Study 3: Communication Link Failure Resiliency

In Study 3, Load 4 is always disconnected from the system, while Loads 1–3 are connected to the system. Under this circumstance, the active and reactive powers of Load 3 are 46.4% and 100% of the whole active power and reactive power loads, respectively. The system is operated under the three-layer controls. At $t = t_5$, a communication link failure in the lower communication network happens, i.e., the link from DG_{22} to DG_{21} fails. Subsequently, at $t = t_6$, Load 3 is switched OFF. Then, at $t = t_7$, a communication link failure in the upper communication network happens, i.e., the link from MG_2 agent to MG_1 agent fails. Finally, at $t = t_8$, Load 3 is switched ON again. Fig. 14 shows that the control objectives in terms of system frequency, system critical bus voltage, GCIV, and reactive power sharing can still be realized after communication link failures. This is because the remaining communication network still contains a spanning tree, and, thus, the convergence condition of algorithms in (1) and (2) is still satisfied.

Remark 5: Switching ON and OFF Load 3 corresponds to a large load disturbance to the system. The results of Fig. 14 show that no significant overshoots are observed, and the inverters are not tripped. Therefore, the robustness of our control method against large load disturbances can be validated.

VII. Conclusion

This article presents a pinning-based hierarchical and distributed cooperative control strategy for AC MGC. The proposed method fully reserves the autonomy characteristic of each individual MG while realizing their coordination through pinning links and communications among MG agents in the upper cyber network.

With the proposed method, multiple control objectives can be achieved, including minimization of the system overall generation cost, restoration of system frequency and critical bus voltage, voltage control capability for the PCC bus of each MG, and an accurate reactive power sharing among DG units in the whole system.

In addition, this article also develops a unified small-signal dynamic model for AC MGC to analyze the system small-signal stability. The model captures the details of the three-layer controllers of DGs and MGs, and also considers the circuit features of networks and loads. Eigen-analysis results reveal that the dominant oscillation modes are associated with different control layers and the interaction among control layers may lead to low-damping modes, and the relation between dominant oscillatory modes and control parameters exhibits complex multivariate interactions.

Finally, the performance of the proposed method is evaluated and validated by time-domain simulation and experimental results.

APPENDIX A
PARAMETERS OF THE DOUBLE-LAYER CYBER NETWORK

The associated adjacency matrix and leader-adjacency matrix parameters for Fig. 4 are given by

$$\widetilde{\mathcal{A}} = \begin{bmatrix} 0 & 1 & 1 \\ 1 & 0 & 1 \\ 1 & 1 & 0 \end{bmatrix} \quad \mathcal{A}^1 = \begin{bmatrix} 0 & 1 & 1 \\ 1 & 0 & 1 \\ 1 & 1 & 0 \end{bmatrix}$$

$$\mathcal{A}^2 = \begin{bmatrix} 0 & 1 & 1 \\ 1 & 0 & 1 \\ 1 & 1 & 0 \end{bmatrix} \quad \mathcal{A}^3 = \begin{bmatrix} 0 & 1 & 1 \\ 1 & 0 & 1 \\ 1 & 1 & 0 \end{bmatrix}$$

$$\mathcal{B}^1_{\text{pin}} = \mathcal{B}^2_{\text{pin}} = \mathcal{B}^3_{\text{pin}} = \begin{bmatrix} 1 & 0 & 0 \end{bmatrix}. \tag{57}$$

APPENDIX B
DETAILED SMALL-SIGNAL DYNAMIC MODELING PROCESS IN SECTION IV

This appendix provides details of the small-signal dynamic modeling process and parameter matrices in Section IV. Denote N as the number of all the DG units in the MGC system, i.e., $N = \sum_{k=1}^{M} N_k$. The generation cost function $\text{GC}_{ki}(P_{ki})$ is assumed to be the quadratic function in (56). Therefore, we have $\eta_{ki}(P_{ki}) = 2\alpha_{ki}P_{ki} + \beta_{ki}$.

Linearizing (11) yields

$$\Delta\omega_{ki} = C_{pw}\begin{bmatrix} \Delta\delta_{ki} \\ \Delta P_{ki} \\ \Delta Q_{ki} \end{bmatrix} + \Delta\Omega_{ki}$$

$$C_{pw} = \begin{bmatrix} 0 & -2k_{ed}\alpha_{ki} & 0 \end{bmatrix}. \tag{58}$$

In light of (58), linearizing (12) yields

$$\Delta\dot{\Omega}_{ki} = A_f\begin{bmatrix} \Delta\delta_{ki} \\ \Delta P_{ki} \\ \Delta Q_{ki} \end{bmatrix} + B_f\Delta\Omega_{ki} + c_{\omega ki}\sum_{j\in\mathcal{N}_i^k} a_{ij}^k\Delta\Omega_{kj}$$
$$- 2\left(c_{\omega ki} - c_{Pki}\right)\sum_{j\in\mathcal{N}_i^k} a_{ij}^k k_{ed}\alpha_{kj}\Delta P_{kj}$$
$$+ c_{\omega ki}g_i^k\Delta\omega_{\text{ref}k}$$

$$A_f = \begin{bmatrix} 0 & 2\left(\left(c_{\omega ki} - c_{Pki}\right)\sum_{j\in\mathcal{N}_i^k} a_{ij}^k + c_{\omega ki}g_i^k\right)k_{ed}\alpha_{ki} & 0 \end{bmatrix}$$

$$B_f = -c_{\omega ki}\left(\sum_{j\in\mathcal{N}_i^k} a_{ij}^k + g_i^k\right). \tag{59}$$

From (13a), we have

$$V_{fki} = V_n - n_{ki}Q_{ki} + \lambda_{ki}. \tag{60}$$

Linearizing (14) and (60) and rearranging the linearized results yield

$$\Delta\dot{\lambda}_{ki} = A_g\begin{bmatrix} \Delta\delta_{ki} \\ \Delta P_{ki} \\ \Delta Q_{ki} \end{bmatrix} + B_g\Delta\lambda_{ki} - c_{vki}\sum_{j\in\mathcal{N}_i^k} a_{ij}^k n_{kj}\Delta Q_{kj}$$
$$+ c_{vki}\sum_{j\in\mathcal{N}_i^k} a_{ij}^k\Delta\lambda_{kj} + c_{vki}g_i^k\Delta V_{\text{ref}k}$$

$$A_g = \begin{bmatrix} 0 & 0 & c_{vki}\left(\sum_{j\in\mathcal{N}_i^k} a_{ij}^k + g_i^k\right)n_{ki} \end{bmatrix}$$

$$B_g = -c_{vki}\left(\sum_{j\in\mathcal{N}_i^k} a_{ij}^k + g_i^k\right). \tag{61}$$

By linearizing (15), we have

$$\Delta\dot{h}_{ki} = A_h\begin{bmatrix} \Delta\delta_{ki} \\ \Delta P_{ki} \\ \Delta Q_{ki} \end{bmatrix} - c_{Qki}\sum_{j\in\mathcal{N}_i^k} a_{ij}^k n_{kj}\Delta Q_{kj}$$

$$A_h = \begin{bmatrix} 0 & 0 & c_{Qki}\sum_{j\in\mathcal{N}_i^k} a_{ij}^k n_{kj} \end{bmatrix}. \tag{62}$$

Based on the instantaneous power theory, the instantaneous output active power $\tilde{p}_{ki}$ and reactive power $\tilde{q}_{ki}$ of DG_{ki} are expressed as

$$\tilde{p}_{ki} = v_{odki}i_{odki} + v_{oqki}i_{oqki} \tag{63a}$$

$$\tilde{q}_{ki} = v_{odki}i_{oqki} - v_{oqki}i_{odki}. \tag{63b}$$

The average active power P_{ki} and reactive power Q_{ki} can be obtained based on first-order low-pass filters, i.e.

$$P_{ki} = \frac{\omega_c}{s+\omega_c}\tilde{p}_{ki} \tag{64a}$$

$$Q_{ki} = \frac{\omega_c}{s+\omega_c}\tilde{q}_{ki} \tag{64b}$$

where ω_c is the cutoff frequency of the first-order low-pass filter $\frac{\omega_c}{s+\omega_c}$ and it is set as 100 rad/s for the numerical and experimental studies in this article.

By linearizing (25), (63), and (64) and substituting (58) into the linearized results, we have

$$\begin{bmatrix} \Delta\dot{\delta}_{ki} \\ \Delta\dot{P}_{ki} \\ \Delta\dot{Q}_{ki} \end{bmatrix} = A_P\begin{bmatrix} \Delta\delta_{ki} \\ \Delta P_{ki} \\ \Delta Q_{ki} \end{bmatrix} + D_P\Delta\Omega_{ki} + B_{P1}\left[\Delta v_{odqki}\right]$$
$$+ B_{P2}\left[\Delta i_{odqki}\right] + C_P\Delta\omega_g$$

$$A_P = \begin{bmatrix} 0 & -2k_{ed}\alpha_{ki} & 0 \\ 0 & -\omega_c & 0 \\ 0 & 0 & -\omega_c \end{bmatrix} \quad C_P = \begin{bmatrix} -1 \\ 0 \\ 0 \end{bmatrix}$$

$$B_{P1} = \begin{bmatrix} 0 & 0 \\ \omega_c I_{odki} & \omega_c I_{oqki} \\ -\omega_c I_{oqki} & \omega_c I_{odki} \end{bmatrix} \quad D_P = \begin{bmatrix} 1 \\ 0 \\ 0 \end{bmatrix}$$

$$B_{P2} = \begin{bmatrix} 0 & 0 \\ \omega_c V_{odki} & \omega_c V_{oqki} \\ \omega_c V_{oqki} & -\omega_c V_{odki} \end{bmatrix} \tag{65}$$

where $V_{odki}, V_{oqki}, I_{odki}$, and I_{oqki} are the equilibrium point values of $v_{odki}, v_{oqki}, i_{odki}$, and i_{oqki} for linearization.

Recall (26). Linearizing (13) yields

$$\Delta v_{odqki} = C_{PV}\begin{bmatrix}\Delta\delta_{ki}\\ \Delta P_{ki}\\ \Delta Q_{ki}\end{bmatrix} + D_{PV1}\Delta\lambda_{ki} + D_{PV2}\Delta h_{ki}$$

$$C_{PV} = \begin{bmatrix}0 & 0 & -n_{ki}\\ 0 & 0 & 0\end{bmatrix}\quad D_{PV1} = \begin{bmatrix}1\\ 0\end{bmatrix}$$

$$D_{PV2} = \begin{bmatrix}-1\\ 0\end{bmatrix}. \tag{66}$$

The DG unit output voltage v_{odqki} and current i_{odqki} are expressed in the local dq reference frame of DG$_{ki}$. To integrate DG$_{ki}$ into the whole system model, v_{odqki} and i_{odqki} need to be transformed to the form in the global DQ-frame, i.e., v_{oDQki} and i_{oDQki}. The transformation is given by

$$\Delta v_{oDQki} = T_s\Delta v_{odqki} + T_c\Delta\delta_{ki} \tag{67}$$

$$\Delta i_{odqki} = T_s^{-1}\Delta i_{oDQki} + T_V^{-1}\Delta\delta_{ki} \tag{68}$$

$$T_s = \begin{bmatrix}\cos\delta_{0ki} & -\sin\delta_{0ki}\\ \sin\delta_{0ki} & \cos\delta_{0ki}\end{bmatrix}$$

$$T_c = \begin{bmatrix}-V_{odki}\sin\delta_{0ki} - V_{oqki}\cos\delta_{0ki}\\ V_{odki}\cos\delta_{0ki} - V_{oqki}\sin\delta_{0ki}\end{bmatrix}$$

$$T_V^{-1} = \begin{bmatrix}-I_{oDki}\sin\delta_{0ki} + I_{oQki}\cos\delta_{0ki}\\ -I_{oDki}\cos\delta_{0ki} - I_{oQki}\sin\delta_{0ki}\end{bmatrix} \tag{69}$$

where δ_{0ki} is the equilibrium point value of δ_{ki}.

Then, the small-signal dynamic model of DG$_{ki}$, i.e., (27), can be obtained by substituting (66) and (68) into (65), and combining the substituted results and (59), (61), and (62). Details of the parameter matrices in (27) are provided in (80) shown at the bottom of the next page. Moreover, from (58), we have

$$\Delta\omega_{ki} = D_{\text{inv}ki}\Delta X_{\text{inv}ki}$$

$$D_{\text{inv}ki} = \begin{bmatrix}C_{pw} & 1 & 0 & 0\end{bmatrix}_{1\times 6} \tag{70}$$

$$\Delta\omega_g = D_{\text{INV1}}\Delta X_{\text{INV1}}$$

$$D_{\text{INV1}} = \begin{bmatrix}D_{\text{inv}11} & 0 & \dots & 0\end{bmatrix}_{1\times 6N_1}. \tag{71}$$

Thus, D_{INV} in (39) is

$$D_{\text{INV}} = \begin{bmatrix}D_{\text{INV1}} & 0 & \dots & 0\end{bmatrix}_{1\times 6N}. \tag{72}$$

Details of the parameter matrices in the small-signal dynamic model of MG$_k$, i.e., (29), are provided in (81), shown at the bottom of the next page.

Substituting (66) into (67) yields

$$\Delta v_{oDQki} = L_{\text{inv}ki}\Delta X_{\text{inv}ki}$$

$$L_{\text{inv}ki} = \begin{bmatrix}T_sC_{PV} + \widetilde{T}_c & 0 & T_sD_{PV1} & T_sD_{PV2}\end{bmatrix}_{2\times 6}$$

$$\widetilde{T}_c = \begin{bmatrix}T_c & 0 & 0\end{bmatrix}. \tag{73}$$

Then, $L_{\text{INV}k}$ and L_{INV} in (30) and (31) can be expressed as

$$L_{\text{INV}k} = \begin{bmatrix}L_{\text{inv}k1} & 0 & \dots & 0\\ 0 & L_{\text{inv}k2} & \dots & 0\\ \vdots & \vdots & \ddots & \vdots\\ 0 & 0 & \dots & L_{\text{inv}kN_k}\end{bmatrix}_{2N_k\times 6N_k}$$

$$L_{\text{INV}} = \begin{bmatrix}L_{\text{INV1}} & 0 & \dots & 0\\ 0 & L_{\text{INV2}} & \dots & 0\\ \vdots & \vdots & \ddots & \vdots\\ 0 & 0 & \dots & L_{\text{INV}M}\end{bmatrix}_{2N\times 6N}. \tag{74}$$

In (36) and (37), $A_{\text{PCC}k} = [\,\frac{V_{\text{PCCD}k0}}{V_{\text{PCC}k0}}\ \frac{V_{\text{PCCQ}k0}}{V_{\text{PCC}k0}}\,]$, where $V_{\text{PCCD}k0}$, $V_{\text{PCCQ}k0}$, and $V_{\text{PCC}k0}$ are the equilibrium point values of $V_{\text{PCCD}k}$, $V_{\text{PCCQ}k}$, and $V_{\text{PCC}k}$.

Details of the parameter matrices in the combination model of all individual MGs in (40) and (41) and the state-space equation of $\Delta\overline{\psi}$ (42) are provided in (82) shown at the top of the page 19.

For the MGC-layer controller of MG$_k$ agent, linearizing (18) and (19) yields

$$\begin{aligned}\Delta\dot{\Phi}_k = {} & B_{cf}\Delta\Phi_k + c_{\omega k}\sum_{l\in\mathcal{H}^k}\tilde{a}_{kl}\Delta\Phi_l\\ & - c_{Pk}\sum_{l\in\mathcal{H}^k}\tilde{a}_{kl}\left(\frac{1}{|\mathcal{F}^k|}\sum_{i\in\mathcal{F}^k}2\alpha_{ki}\Delta P_{ki}\right)\\ & + c_{Pk}\sum_{l\in\mathcal{H}^k}\tilde{a}_{kl}\left(\frac{1}{|\mathcal{F}^l|}\sum_{i\in\mathcal{F}^l}2\alpha_{li}\Delta P_{li}\right)\\ B_{cf} = {} & -c_{\omega k}\left(\sum_{l\in\mathcal{H}^k}\tilde{a}_{kl} + \tilde{g}_k\right).\end{aligned} \tag{75}$$

Linearizing (21) and (43) yields

$$\Delta\dot{T}_k = B_{cg}\Delta T_k + c_{vk}\sum_{l\in\mathcal{H}^k}\tilde{a}_{kl}\Delta T_l + c_{vk}\tilde{g}_k\Delta V_{\text{sref}}$$

$$B_{cg} = -c_{vk}\left(\sum_{l\in\mathcal{H}^k}\tilde{a}_{kl} + \tilde{g}_k\right). \tag{76}$$

Linearizing (23) yields

$$\begin{aligned}\Delta\dot{H}_k = {} & c_{Qk}\sum_{l\in\mathcal{H}^k}\tilde{a}_{kl}\left(\frac{1}{|\mathcal{F}^k|}\sum_{i\in\mathcal{F}^k}n_{ki}\Delta Q_{ki}\right)\\ & - c_{Qk}\sum_{l\in\mathcal{H}^k}\tilde{a}_{kl}\left(\frac{1}{|\mathcal{F}^l|}\sum_{i\in\mathcal{F}^l}n_{li}\Delta Q_{li}\right).\end{aligned} \tag{77}$$

Then, (44) can be obtained by combining (75), (76), and (77). The details of $A_{\text{MGC}k}$, $F_{\text{MGC}kl}$, and $H_{\text{MGC}k}$ are given by

$$A_{\text{MGC}k} = \begin{bmatrix}B_{cf} & 0 & 0\\ 0 & B_{cg} & 0\\ 0 & 0 & 0\end{bmatrix}_{3\times 3}\quad H_{\text{MGC}k} = \begin{bmatrix}0\\ c_{vk}\tilde{g}_k\\ 0\end{bmatrix}_{3\times 1}$$

$$F_{\mathrm{MGC}kl} = \begin{bmatrix} c_{\omega k}\tilde{a}_{kl} & 0 & 0 \\ 0 & c_{vk}\tilde{a}_{kl} & 0 \\ 0 & 0 & 0 \end{bmatrix}_{3\times 3}. \tag{78}$$

$E_{\mathrm{MGC}k}$ is a $3 \times 6N$ sparse matrix. For the first row of $E_{\mathrm{MGC}k}$, the elements corresponding to ΔP_{ki} of the pinned DG units of MG_k are $-c_{Pk}\sum_{l\in\mathcal{H}^k}\tilde{a}_{kl}\frac{2\alpha_{ki}}{|\mathcal{F}^k|}$, and the elements corresponding to ΔP_{li} of the pinned DG units of MG_l are $c_{Pk}\tilde{a}_{kl}\frac{2\alpha_{li}}{|\mathcal{F}^l|}$. The second row of $E_{\mathrm{MGC}k}$ are all zeros. For the third row of $E_{\mathrm{MGC}k}$, the elements corresponding to ΔQ_{ki} of the pinned DG units of MG_k are $c_{Qk}\sum_{l\in\mathcal{H}^k}\tilde{a}_{kl}\frac{n_{ki}}{|\mathcal{F}^k|}$, and the elements corresponding to ΔQ_{li} of the pinned DG units of MG_l are $-c_{Qk}\tilde{a}_{kl}\frac{n_{li}}{|\mathcal{F}^l|}$.

Then, details of the parameter matrices in (45) are provided in (83) shown at the top of the next page.

In (47) and (48), $A_{\mathrm{cri}} = [\,\frac{V_{\mathrm{cri}D0}}{V_{\mathrm{cri}0}}\ \frac{V_{\mathrm{cri}Q0}}{V_{\mathrm{cri}0}}\,]$, where $V_{\mathrm{cri}D0}$, $V_{\mathrm{cri}Q0}$, and $V_{\mathrm{cri}0}$ are the equilibrium point values of $V_{\mathrm{cri}D}$, $V_{\mathrm{cri}Q}$, and V_{cri}.

Details of $A_{\mathrm{cou}} \in \mathbb{R}^{M\times 3M}$ and $B_{\mathrm{cou}} \in \mathbb{R}^{M\times 3M}$ in (53) and (54) are given by

$$A_{\mathrm{cou}} = \begin{bmatrix} A_{yy} & 0 & \dots & 0 \\ 0 & A_{yy} & \dots & 0 \\ \vdots & \vdots & \ddots & \vdots \\ 0 & 0 & \dots & A_{yy} \end{bmatrix} A_{yy} = \begin{bmatrix} 1 & 0 & 0 \end{bmatrix}$$

$$B_{\mathrm{cou}} = \begin{bmatrix} B_{yy} & 0 & \dots & 0 \\ 0 & B_{yy} & \dots & 0 \\ \vdots & \vdots & \ddots & \vdots \\ 0 & 0 & \dots & B_{yy} \end{bmatrix} B_{yy} = \begin{bmatrix} 0 & 1 & -1 \end{bmatrix}. \tag{79}$$

Finally, the detail of A_{sys} in the complete MGC system model in (55) is provided in (84), shown at the top of the next page.

$$A_{\mathrm{inv}ki} = \begin{bmatrix} A_P + B_{P1}C_{PV} + B_{P2}\begin{bmatrix} T_V^{-1} & 0 & 0 \end{bmatrix} & D_P & B_{P1}D_{PV1} & B_{P1}D_{PV2} \\ A_f & B_f & 0 & 0 \\ A_g & 0 & B_g & 0 \\ A_h & 0 & 0 & 0 \end{bmatrix}_{6\times 6}$$

$$B_{\mathrm{inv}ki} = \begin{bmatrix} B_{P2}T_s^{-1} \\ 0 \\ 0 \\ 0 \end{bmatrix}_{6\times 2} \quad C_{\mathrm{inv}ki} = \begin{bmatrix} C_P \\ 0 \\ 0 \\ 0 \end{bmatrix}_{6\times 1} \quad H_{\mathrm{inv}ki} = \begin{bmatrix} 0 \\ 0 \\ c_{vki}g_i^k \\ 0 \end{bmatrix}_{6\times 1} \quad R_{\mathrm{inv}ki} = \begin{bmatrix} 0 \\ c_{\omega ki}g_i^k \\ 0 \\ 0 \end{bmatrix}_{6\times 1}$$

$$F_{\mathrm{inv}kij} = \begin{bmatrix} 0 & 0 & 0 & 0 & 0 & 0 \\ 0 & -2(c_{\omega ki}-c_{Pki})a_{ij}^k k_{ed}\alpha_{kj} & 0 & c_{\omega ki}a_{ij}^k & 0 & 0 \\ 0 & 0 & -c_{vki}a_{ij}^k n_{kj} & 0 & c_{vki}a_{ij}^k & 0 \\ 0 & 0 & -c_{Qki}a_{ij}^k n_{kj} & 0 & 0 & 0 \end{bmatrix}_{6\times 6} \tag{80}$$

$$A_{\mathrm{INV}k} = G_{\mathrm{INV}k} + F_{\mathrm{INV}k}$$

$$G_{\mathrm{INV}k} = \begin{bmatrix} A_{\mathrm{inv}k1} & 0 & \dots & 0 \\ 0 & A_{\mathrm{inv}k2} & \dots & 0 \\ \vdots & \vdots & \ddots & \vdots \\ 0 & 0 & \dots & A_{\mathrm{inv}kN_k} \end{bmatrix}_{6N_k\times 6N_k} \quad F_{\mathrm{INV}k} = \begin{bmatrix} F_{\mathrm{inv}k11} & F_{\mathrm{inv}k12} & \dots & F_{\mathrm{inv}k1N_k} \\ F_{\mathrm{inv}k21} & F_{\mathrm{inv}k22} & \dots & F_{\mathrm{inv}k2N_k} \\ \vdots & \vdots & \ddots & \vdots \\ F_{\mathrm{inv}kN_k1} & F_{\mathrm{inv}kN_k2} & \dots & F_{\mathrm{inv}kN_kN_k} \end{bmatrix}_{6N_k\times 6N_k}$$

$$B_{\mathrm{INV}k} = \begin{bmatrix} B_{\mathrm{inv}k1} & 0 & \dots & 0 \\ 0 & B_{\mathrm{inv}k2} & \dots & 0 \\ \vdots & \vdots & \ddots & \vdots \\ 0 & 0 & \dots & B_{\mathrm{inv}kN_k} \end{bmatrix}_{6N_k\times 2N_k} \quad C_{\mathrm{INV}k} = \begin{bmatrix} C_{\mathrm{inv}k1} \\ C_{\mathrm{inv}k2} \\ \vdots \\ C_{\mathrm{inv}kN_k} \end{bmatrix}_{6N_k\times 1} \quad H_{\mathrm{INV}k} = \begin{bmatrix} H_{\mathrm{inv}k1} \\ H_{\mathrm{inv}k2} \\ \vdots \\ H_{\mathrm{inv}kN_k} \end{bmatrix}_{6N_k\times 1}$$

$$R_{\mathrm{INV}k} = \begin{bmatrix} R_{\mathrm{inv}k1} \\ R_{\mathrm{inv}k2} \\ \vdots \\ R_{\mathrm{inv}kN_k} \end{bmatrix}_{6N_k\times 1} \tag{81}$$

$$A_{\mathrm{INV}}=\begin{bmatrix} A_{\mathrm{INV1}} & 0 & \dots & 0 \\ 0 & A_{\mathrm{INV2}} & \dots & 0 \\ \vdots & \vdots & \ddots & \vdots \\ 0 & 0 & \dots & A_{\mathrm{INV}M} \end{bmatrix}_{6N\times 6N} \quad B_{\mathrm{INV}}=\begin{bmatrix} B_{\mathrm{INV1}} & 0 & \dots & 0 \\ 0 & B_{\mathrm{INV2}} & \dots & 0 \\ \vdots & \vdots & \ddots & \vdots \\ 0 & 0 & \dots & B_{\mathrm{INV}M} \end{bmatrix}_{6N\times 2N}$$

$$H_{\mathrm{INV}}=\begin{bmatrix} H_{\mathrm{INV1}} & 0 & \dots & 0 \\ 0 & H_{\mathrm{INV2}} & \dots & 0 \\ \vdots & \vdots & \ddots & \vdots \\ 0 & 0 & \dots & H_{\mathrm{INV}M} \end{bmatrix}_{6N\times M} \quad R_{\mathrm{INV}}=\begin{bmatrix} R_{\mathrm{INV1}} & 0 & \dots & 0 \\ 0 & R_{\mathrm{INV2}} & \dots & 0 \\ \vdots & \vdots & \ddots & \vdots \\ 0 & 0 & \dots & R_{\mathrm{INV}M} \end{bmatrix}_{6N\times M}$$

$$C_{\mathrm{INV}}=\begin{bmatrix} C_{\mathrm{INV1}} \\ C_{\mathrm{INV2}} \\ \vdots \\ C_{\mathrm{INV}M} \end{bmatrix}_{6N\times 1} \quad N_{\mathrm{INV}}=\begin{bmatrix} H_{\mathrm{INV1}}A_{\mathrm{PCC1}}Z_{\mathrm{PCC1}} \\ H_{\mathrm{INV2}}A_{\mathrm{PCC2}}Z_{\mathrm{PCC2}} \\ \vdots \\ H_{\mathrm{INV}1M}A_{\mathrm{PCC}M}Z_{\mathrm{PCC}M} \end{bmatrix}_{6N\times 2N} \quad T_{\mathrm{PCC}}=\begin{bmatrix} A_{\mathrm{PCC1}}Z_{\mathrm{PCC1}} \\ A_{\mathrm{PCC2}}Z_{\mathrm{PCC2}} \\ \vdots \\ A_{\mathrm{PCC}M}Z_{\mathrm{PCC}M} \end{bmatrix}_{M\times 2N} \tag{82}$$

$$A_{\mathrm{MGC}}=G_{\mathrm{MGC}}+F_{\mathrm{MGC}}$$

$$G_{\mathrm{MGC}}=\begin{bmatrix} A_{\mathrm{MGC1}} & 0 & \dots & 0 \\ 0 & A_{\mathrm{MGC2}} & \dots & 0 \\ \vdots & \vdots & \ddots & \vdots \\ 0 & 0 & \dots & A_{\mathrm{MGC}M} \end{bmatrix}_{3M\times 3M} \quad H_{\mathrm{MGC}}=\begin{bmatrix} H_{\mathrm{MGC1}} \\ H_{\mathrm{MGC2}} \\ \vdots \\ H_{\mathrm{MGC}M} \end{bmatrix}_{3M\times 1}$$

$$F_{\mathrm{MGC}}=\begin{bmatrix} F_{\mathrm{MGC11}} & F_{\mathrm{MGC12}} & \dots & F_{\mathrm{MGC1}M} \\ F_{\mathrm{MGC21}} & F_{\mathrm{MGC22}} & \dots & F_{\mathrm{MGC2}M} \\ \vdots & \vdots & \ddots & \vdots \\ F_{\mathrm{MGC}M1} & F_{\mathrm{MGC}M2} & \dots & F_{\mathrm{MGC}MM} \end{bmatrix}_{3M\times 3M} \quad E_{\mathrm{MGC}}=\begin{bmatrix} E_{\mathrm{MGC1}} \\ E_{\mathrm{MGC2}} \\ \vdots \\ E_{\mathrm{MGC}M} \end{bmatrix}_{3M\times 6N} \tag{83}$$

$$A_{\mathrm{sys}}=\begin{bmatrix} J_{\mathrm{INV}} & k_{\mathrm{I}}H_{\mathrm{INV}} & R_{\mathrm{INV}}A_{\mathrm{cou}}+k_{\mathrm{P}}H_{\mathrm{INV}}B_{\mathrm{cou}} & 0 \\ -T_{\mathrm{PCC}}W_{\mathrm{INV}} & 0 & B_{\mathrm{cou}} & 0 \\ J_{\mathrm{MGC}} & 0 & A_{\mathrm{MGC}} & k_{\mathrm{IS}}H_{\mathrm{MGC}} \\ -A_{\mathrm{cri}}Z_{\mathrm{cri}}W_{\mathrm{INV}} & 0 & 0 & 0 \end{bmatrix}_{(6N+4M+1)\times(6N+4M+1)} \tag{84}$$

REFERENCES

[1] J. M. Guerrero, J. C. Vasquez, J. Matas, D. Vicuna, L. García, and M. Castilla, "Hierarchical control of droop-controlled AC and DC microgrids–A general approach toward standardization," *IEEE Trans. Ind. Electron.*, vol. 58, no. 1, pp. 158–172, Jan. 2011.

[2] Y. W. Li and C.-N. Kao, "An accurate power control strategy for power-electronics-interfaced distributed generation units operating in a low-voltage multibus microgrid," *IEEE Trans. Power Electron.*, vol. 24, no. 12, pp. 2977–2988, Dec. 2009.

[3] H. Jia, Q. Xiao, and J. He, "An improved grid current and DC capacitor voltage balancing method for three-terminal hybrid AC/DC microgrid," *IEEE Trans. Smart Grid*, vol. 10, no. 6, pp. 5876–5888, Nov. 2019.

[4] Y. Han, K. Zhang, H. Li, E. A. A. Coelho, and J. M. Guerrero, "MAS-based distributed coordinated control and optimization in microgrid and microgrid clusters: A comprehensive overview," *IEEE Trans. Power Electron.*, vol. 33, no. 8, pp. 6488–6508, Aug. 2018.

[5] E. Pashajavid, A. Ghosh, and F. Zare, "A multimode supervisory control scheme for coupling remote droop-regulated microgrids," *IEEE Trans. Smart Grid*, vol. 9, no. 5, pp. 5381–5392, Sep. 2018.

[6] Y. Xu, C.-C. Liu, K. P. Schneider, F. K. Tuffner, and D. T. Ton, "Microgrids for service restoration to critical load in a resilient distribution system," *IEEE Trans. Smart Grid*, vol. 9, no. 1, pp. 426–437, Jan. 2018.

[7] Z. Wang, C. Shen, Y. Xu, F. Liu, X. Wu, and C.-C. Liu, "Risk-limiting load restoration for resilience enhancement with intermittent energy resources," *IEEE Trans. Smart Grid*, vol. 10, no. 3, pp. 2507–2522, May 2019.

[8] Y. Wang *et al.*, "Coordinating multiple sources for service restoration to enhance resilience of distribution systems," *IEEE Trans. Smart Grid*, 2019, vol. 10, no. 5, pp. 5781–5793, Sep. 2019.

[9] Z. Xu, P. Yang, Y. Zhang, Z. Zeng, C. Zheng, and J. Peng, "Control devices development of multi-microgrids based on hierarchical structure," *IET Gener., Transmiss. Distrib.*, vol. 10, no. 16, pp. 4249–4256, 2016.

[10] T. John and S. P. Lam, "Voltage and frequency control during microgrid islanding in a multi-area multi-microgrid system," *IET Gener., Transmiss. Distrib.*, vol. 11, no. 6, pp. 1502–1512, 2017.

[11] R. Zamora and A. K. Srivastava, "Multi-layer architecture for voltage and frequency control in networked microgrids," *IEEE Trans. Smart Grid*, vol. 9, no. 3, pp. 2076–2085, May 2018.

[12] N. J. Gil and J. P. Lopes, "Hierarchical frequency control scheme for islanded multi-microgrids operation," in *Proc. IEEE Lausanne Power Tech.*, 2007, pp. 473–478.

[13] A. Bidram, A. Davoudi, F. L. Lewis, and Z. Qu, "Secondary control of microgrids based on distributed cooperative control of multi-agent systems," *IET Gener., Transmiss. Distrib.*, vol. 7, no. 8, pp. 822–831, 2013.
[14] R. O.-Saber, J. A. Fax, and R. M. Murray, "Consensus and cooperation in networked multi-agent systems," *Proc. IEEE*, vol. 95, no. 1, pp. 215–233, Jan. 2007.
[15] J. W. Simpson-Porco, Q. Shafiee, F. Dörfler, J. C. Vasquez, J. M. Guerrero, and F. Bullo, "Secondary frequency and voltage control of islanded microgrids via distributed averaging," *IEEE Trans. Ind. Electron.*, vol. 62, no. 11, pp. 7025–7038, Nov. 2015.
[16] V. Nasirian, Q. Shafiee, J. Guerrero, F. Lewis, and A. Davoudi, "Droop-free distributed control for AC microgrids," *IEEE Trans. Power Electron.*, vol. 31, no. 2, pp. 1600–1617, Feb. 2016.
[17] V. Nasirian, S. Moayedi, A. Davoudi, and F. L. Lewis, "Distributed cooperative control of DC microgrids," *IEEE Trans. Power Electron.*, vol. 30, no. 4, pp. 2288–2303, Apr. 2015.
[18] Q. Shafiee, J. M. Guerrero, and J. C. Vasquez, "Distributed secondary control for islanded microgrids–A novel approach," *IEEE Trans. Power Electron.*, vol. 29, no. 2, pp. 1018–1031, Feb. 2014.
[19] D. O. Amoateng, M. Al Hosani, M. S. Elmoursi, K. Turitsyn, and J. L. Kirtley, "Adaptive voltage and frequency control of islanded multi-microgrids," *IEEE Trans. Power Syst.*, vol. 33, no. 4, pp. 4454–4465, Jul. 2018.
[20] M. S. Golsorkhi, D. J. Hill, and H. R. Karshenas, "Distributed voltage control and power management of networked microgrids," *IEEE J. Emerg. Sel. Topics Power Electron.*, vol. 6, no. 4, pp. 1892–1902, Dec. 2018.
[21] X. Wu *et al.*, "A two-layer distributed cooperative control method for islanded networked microgrid systems," *IEEE Trans. Smart Grid*, to be published, doi: 10.1109/TSG.2019.2928330.
[22] X. Lu, J. Lai, X. Yu, Y. Wang, and J. M. Guerrero, "Distributed coordination of islanded microgrid clusters using a two-layer intermittent communication network," *IEEE Trans. Ind. Informat.*, vol. 14, no. 9, pp. 3956–3969, Sep. 2018.
[23] S. Moayedi and A. Davoudi, "Distributed tertiary control of DC microgrid clusters," *IEEE Trans. Power Electron.*, vol. 31, no. 2, pp. 1717–1733, Feb. 2016.
[24] Q. Shafiee, T. Dragičević, J. C. Vasquez, and J. M. Guerrero, "Hierarchical control for multiple DC-microgrids clusters," *IEEE Trans. Energy Convers.*, vol. 29, no. 4, pp. 922–933, Dec. 2014.
[25] J. Lai, X. Lu, X. Yu, and A. Monti, "Cluster-oriented distributed cooperative control for multiple AC microgrids," *IEEE Trans. Ind. Informat.*, vol. 15, no. 11, pp. 5906–5918, Nov. 2019.
[26] N. Pogaku, M. Prodanović, and T. C. Green, "Modeling, analysis and testing of autonomous operation of an inverter-based microgrid," *IEEE Trans. Power Electron.*, vol. 22, no. 2, pp. 613–625, Mar. 2007.
[27] X. Wu, C. Shen, and R. Iravani, "A distributed, cooperative frequency and voltage control for microgrids," *IEEE Trans. Smart Grid*, vol. 9, no. 4, pp. 2764–2776, Jul. 2018.
[28] X. Wu and C. Shen, "Distributed optimal control for stability enhancement of microgrids with multiple distributed generators," *IEEE Trans. Power Syst.*, vol. 32, no. 5, pp. 4045–4059, Sep. 2017.
[29] N. Bottrell, M. Prodanovic, and T. C. Green, "Dynamic stability of a microgrid with an active load," *IEEE Trans. Power Electron.*, vol. 28, no. 11, pp. 5107–5119, Nov. 2013.
[30] H. Liang, B. J. Choi, W. Zhuang, and X. Shen, "Stability enhancement of decentralized inverter control through wireless communications in microgrids," *IEEE Trans. Smart Grid*, vol. 4, no. 1, pp. 321–331, Mar. 2013.
[31] G. Chen and E. Feng, "Distributed secondary control and optimal power sharing in microgrids," *IEEE/CAA J. Automatica Sinica*, vol. 2, no. 3, pp. 304–312, Jul. 2015.

Xiangyu Wu (Member, IEEE) received the B.S. degree from the Department of Electrical Engineering, Zhejiang University, Hangzhou, China, in 2012, and the Ph.D. degree in electrical engineering from Tsinghua University, Beijing, China, in 2017.

He is currently a Postdoctoral Researcher with the School of Electrical Engineering, Beijing Jiaotong University, Beijing, China. In 2015, he was a Visiting Scholar with the University of Toronto, Toronto, ON, Canada. In 2019, he was a Guest Researcher with the Department of Energy Technology, Aalborg University, Aalborg, Denmark. His research interests include the control and stability analysis of microgrids and power electronic-based power systems.

Yin Xu (Senior Member, IEEE) received the B.E. and Ph.D. degrees in electrical engineering from Tsinghua University, Beijing, China, in 2008 and 2013, respectively.

He is currently a Professor with the School of Electrical Engineering, Beijing Jiaotong University, Beijing, China. From 2013 to 2016, he was an Assistant Research Professor with the School of Electrical Engineering and Computer Science, Washington State University, Pullman, WA, USA. His research interests include power system resilience, distribution system restoration, power system electromagnetic transient simulation, and ac–dc hybrid power systems.

Dr. Xu is currently serving as the Secretary of the Distribution Test Feeder Working Group under the IEEE PES Distribution System Analysis Subcommittee.

Jinghan He (Fellow, IEEE) received the M.Sc. degree in electrical engineering from Tianjin University, Tianjin, China, in 1994, and the Ph.D. degree in electrical engineering from Beijing Jiaotong University, Beijing, China, in 2007.

She is currently a Professor with Beijing Jiaotong University, Beijing, China. Her main research interests include protective relaying, fault distance measurement, and location in power systems.

Xiaojun Wang (Member, IEEE) received the B.S., M.Sc., and Ph.D. degrees from the North China Electric Power University, Beijing, China, in 2001, 2004, and 2008, respectively.

In 2014, he was a Bond Scheme Scholar with ALTOM Grid, Stafford, U.K. He is currently an Associate Professor with Beijing Jiaotong University, Beijing, China. His main research interests include planning and operation of integrated energy systems, the application of machine learning in power system operations, and fault location.

Juan C. Vasquez (Senor Member, IEEE) received the B.S. degree in electronics engineering from the Autonomous University of Manizales, Manizales, Colombia in 2004, and the Ph.D. degree in automatic control, robotics, and computer vision from BarcelonaTech-UPC, Barcelona, Spain, in 2009.

In 2011, he was an Assistant Professor with the Department of Energy Technology, Aalborg University, Aalborg, Denmark, where he became an Associate Professor in 2014. In 2019, he became a Professor in Energy Internet and Microgrids and is currently the Co-Director of the Villum Center for Research on Microgrids. He was a Visiting Scholar with the Center of Power Electronics Systems, Virginia Tech, Blacksburg, VA, USA, and a Visiting Professor with Ritsumeikan University, Kyoto, Japan. He has published more than 450 journal papers in the field of microgrids, which, in total, are cited more than 19 000 times. His current research interests include operation, advanced hierarchical and cooperative control, optimization and energy management applied to distributed generation in ac–dc microgrids, maritime microgrids, advanced metering infrastructures and the integration of Internet of Things and Energy Internet into the SmartGrid.

Prof. Vasquez is an Associate Editor of *IET Power Electronics* and a Guest Editor of the IEEE TRANSACTIONS ON INDUSTRIAL INFORMATICS Special Issue on Energy Internet. He received the Highly Cited Researcher Award by Thomson Reuters from 2017 to 2019, and the Young Investigator Award 2019. He is currently a member of the IEC System Evaluation Group SEG4 on LVDC Distribution and Safety for use in Developed and Developing Economies, the Renewable Energy Systems Technical Committee TC-RES in IEEE Industrial Electronics, PELS, IAS, and PES Societies.

Josep M. Guerrero (Fellow, IEEE) received the B.S. degree in telecommunications engineering, the M.S. degree in electronics engineering, and the Ph.D. degree in power electronics from the Technical University of Catalonia, Catalonia, Barcelona, in 1997, 2000, and 2003, respectively.

Since 2011, he has been a Full Professor with the Department of Energy Technology, Aalborg University, Aalborg, Denmark, where he is responsible for the Microgrid Research Program. Since 2014, he has been the Chair Professor with Shandong University, Jinan, China. Since 2015, he is a distinguished Guest Professor with Hunan University, Changsha, China. Since 2016, he has been a Visiting Professor Fellow with Aston University, Birmingham, U.K., and a Guest Professor with the Nanjing University of Posts and Telecommunications, Nanjing, China. In 2019, he became a Villum Investigator by The Villum Foundation, which supports the Centre for Research on Microgrids, Aalborg University, where he is also the Founder and Director. He has published more than 500 journal papers in the fields of microgrids and renewable energy systems, which are cited more than 30 000 times. He is specially focused on maritime microgrids for electrical ships, vessels, ferries, and seaports. His research interests include different microgrid aspects, including power electronics, distributed energy-storage systems, hierarchical and cooperative control, energy management systems, smart metering and the Internet of Things for ac–dc microgrid clusters, and islanded minigrids.

Prof. Guerrero is an Associate Editor for several of IEEE Transactions. He received the Best Paper Award of the IEEE TRANSACTIONS ON ENERGY CONVERSION for the period 2014–2015, and the Best Paper Prize of IEEE-PES in 2015. He also received the Best Paper Award of the *Journal of Power Electronics* in 2016. From 2014 to 2018, he was awarded by Clarivate Analytics (former Thomson Reuters) as the Highly Cited Researcher. In 2015, he was promoted as IEEE Fellow for his contributions on distributed power systems and microgrids.